Microbiome

RESEARCH

Open Access

ACE2 shedding exacerbates sepsis-induced gut leak via loss of microbial metabolite 5-methoxytryptophan

Jiacheng Gong[1,2†], Haoyang Lu[1,2†], Yuhan Li[6†], Qihan Xu[1,2†], Yuanyuan Ma[3], Anni Lou[1], Wanfu Cui[1], Weihua Song[1], Peng Qu[1,2], Zhuoer Chen[1,2], Linghao Quan[1,2], Xi Liu[4*], Ying Meng[5*] and Xu Li[1,2*]

Abstract

Background Sepsis, a critical organ dysfunction resulting from an aberrant host response to infection, remains a leading cause of mortality in ICU patients. Recent evidence suggests that angiotensin-converting enzyme 2 (ACE2) contributes to intestinal barrier function, the mechanism of which is yet to be explored. Additionally, alterations in intestinal microbiota and microbial metabolites could affect gut homeostasis, thus playing a potential role in modulating sepsis progression.

Results ACE2 shedding weakens the integrity of the intestinal barrier in sepsis. Mice deficient in ACE2 exhibited increased intestinal permeability and higher mortality rates post-operation compared to their wild-type counterparts. Notably, ACE2 deficiency was associated with distinct alterations in gut microbiota composition and reductions in protective metabolites, such as 5-methoxytryptophan (5-MTP). Supplementing septic mice with 5-MTP ameliorated gut leak through enhanced epithelial cell proliferation and repair. The PI3K-AKT-WEE1 signaling pathway was identified as a key mediator of the beneficial effects of 5-MTP administration.

Conclusion ACE2 plays a protective role in maintaining intestinal barrier function during sepsis, potentially through modulation of the gut microbiota and the production of key metabolite 5-MTP. Our study enriched the mechanisms by which ACE2 regulates gut homeostasis and shed light on further applications.

Keywords Gut leak, Sepsis, Bacterial metabolite, 5-methoxytryptophan, Angiotensin-converting enzyme 2

†Jiacheng Gong, Haoyang Lu, Yuhan Li, and Qihan Xu contributed equally to this work.

*Correspondence:
Xi Liu
haojin_cq@163.com
Ying Meng
nfyymengy@163.com
Xu Li
mylx99@smu.edu.cn
[1] Department of Emergency Medicine, Nanfang Hospital, Southern Medical University, Guangzhou 510515, China
[2] Guangdong Provincial Key Laboratory of Gastroenterology, Department of Gastroenterology, Nanfang Hospital, Southern Medical University, Guangzhou 510515, China
[3] State Key Laboratory of Organ Failure Research, National Clinical Research Center of Kidney Disease, Division of Nephrology, Nanfang Hospital, Southern Medical University, Guangzhou 510515, China
[4] The Third Affiliated Hospital, Guangzhou Medical University, Guangzhou 510515, China
[5] Department of Respiratory Diseases, Nanfang Hospital, Southern Medical University, Guangzhou 510515, China
[6] The Second School of Clinical Medicine, Southern Medical University, Guangzhou 510515, China

Background

Sepsis is defined as a life-threatening organ dysfunction resulting from a dysregulated host response to infection [1]. It is considered one of the major public health issues, leading to substantial mortality among hospitalized patients and enormous healthcare costs [2–4]. As an individualized treatment scheme including effective hemodynamic stabilization and immune response handling is difficult to access, applicable therapeutic methods are in urgent need.

It is becoming increasingly evident that sepsis has a detrimental impact on the intestinal epithelial barrier, which may contribute to the development of organ failure. The intestinal epithelial barrier is comprised of three distinct layers: a physical barrier, a chemical barrier, and a biological barrier. Dysfunction of the intestinal barrier may facilitate the translocation of bacteria and endotoxins, further aggravating multi-organ failure and systemic inflammation [5]. Thus, the control of bacterial translocation has an important impact on mortality in sepsis [6]. These observations indicate that strategies aimed at maintaining intestinal barrier function may prove to be a promising avenue for the prevention and treatment of diseases.

The gut microbiota has emerged as a key factor in the maintenance of the intestinal mechanical barrier, with a role in the maturation of the local and immune systems, as well as in the regulation of epithelial cell proliferation [7, 8]. A number of studies have reported disturbances in the microbiota, which are associated with system infection [9, 10].

Among the various influencing factors, the angiotensin-converting enzyme 2 (ACE2) has aroused our interest because of its multifunctionality. Its enzymatic role in metabolizing angiotensin (Ang) II has been well studied. Another distinct role is in maintaining the intestinal barrier and regulating intestinal flora [11]. Hashimoto et al. demonstrated that loss of ACE2 led to malfunction of the intestinal amino acid transporter B0 AT1, which in turn affected the gut microbiome and increased susceptibility to colitis [12]. Furthermore, the significance of ACE2 in maintaining the integrity of the intestinal epithelial barrier and the composition of the intestinal flora has been corroborated in research on diabetes [13, 14]. However, the mechanism by which ACE2 helps maintain the gut barrier and the interaction between altered microbiome and intestinal homeostasis remain to be elucidated.

As previously stated, numerous gut microbiota have been identified as influencing host physiology, including intestinal homeostasis. However, only a limited number of microbiota-derived metabolites have been characterized [15]. 5-Methoxytryptophan (5-MTP), a novel compound derived from L-tryptophan, has been demonstrated to possess anti-inflammatory properties in the context of systemic inflammation [16] and antifibrotic actions in chronic kidney disease [17]. 5-MTP is produced in vascular cells, pulmonary cells, and renal epithelial cells via two enzymes, hydroxyindole O-methyltransferase (HIOMT), and tryptophan hydroxylase (TPH) [16, 18].

In this study, we conducted a comprehensive evaluation of the functions and mechanisms of ACE2 in regulating intestinal homeostasis in the context of sepsis. Our findings may provide a viable therapeutic approach to limit the severity of sepsis.

Methods

Human specimens

Patients diagnosed with sepsis, presenting with suspected infection and a total Sequential Organ Failure Assessment (SOFA) score of ≥ 2, were recruited (sepsis-3 criteria). Exclusion criteria included pregnancy, cancer, HIV infection, age under 18, and those discharged or deceased within 12 h of admission. Serum samples were collected within 12 h of admission, and relevant medical test results were recorded. Serum samples were also collected from healthy volunteers, who were demographically similar to the septic patients. All samples were centrifuged at 2000 rpm for 10 min at 4 °C and stored at − 80 °C before use.

Enzyme-linked immunosorbent assay

The enzyme-linked immunosorbent assay (ELISA) kit for angiotensin I converting enzyme 2 (SEB886Hu, SEB886Mu, Cloudclone), human lipopolysaccharide-binding protein (CSB-E09629 h, CUSABIO), mouse tumor necrosis factor (CSB-E04741 m, CUSABIO), mouse procalcitonin (CSB-E10371 m, CUSABIO), and mouse serum creatinine (No.2 M-KMLJM219960 m, CAMILO) were utilized following the manufacturer's protocols. Standards of varying concentrations and serum samples were added to the plates, followed by incubation at 37 °C for 1 h. Diluted enzyme-labeled antibodies were subsequently added and incubated for another hour at 37 °C. Then, 90 μL of the substrate solution was added to each well, which was then incubated in the dark at 37 °C for 15 min. The reaction was stopped, and optical density (OD) values were measured at 450 nm.

Measurement of glycemia

Serum glucose levels were measured using a glucose assay kit with O-toluidine. Standards and serum samples were added with glucose assay reagent to achieve a final volume of 190 μL. Vortex thoroughly and centrifuge briefly at 5000 × g to collect the solution. Incubate

the tubes at 95 °C for 8 min in a PCR thermocycler, then cool to 4 °C. Transfer the supernatant from each tube to a 96-well plate and measure the absorbance at 630 nm using a microplate reader.

Animals

Male C57BL/6 and ICR mice, aged 6–8 weeks, were acquired from Guangdong Ruge Biotechnology Co., Ltd., and Guangdong Medical Animal Experimental Center. Both ACE2-knockout mice ($Ace2^{-/y}$ or KO) and h-ACE2 overexpression mice ($hACE2^{+/+}$ or OE) were purchased from VIEWSOLID BIOTECH. The knockout site was selected to be exon7 of the transcription product 202, and the target gene was shifted from exon7 by CRISPR/Cas9 editing [19]. OE mice were generated by microinjection of the mouse Ace2 promoter driving the human ACE2 coding sequence into the pronuclei of fertilized ova from ICR mice [20]. Littermate mice were produced by breeding trios consisting of one $Ace2^{-/y}$ male with two heterozygous females ($ACE2^{\pm}$). Male offspring were genotyped (either $ACE2^{-/y}$ or $ACE2^{+/y}$) and housed in separate cages accordingly after weaning. Mice were housed in a specific pathogen-free (SPF) environment at the Experimental Animal Center of Southern Medical University, maintained at a temperature of 20–25 °C and a relative humidity of 40–70%, with ad libitum access to food and water.

Cecal ligation and puncture

Polymicrobial sepsis was induced by cecal ligation and puncture (CLP) as described [21]. Briefly, mice were anesthetized with 1% pentobarbital, followed by aseptic preparation. A 1.5 cm midline abdominal incision was made to exteriorize the cecum, and 2/3 of the distal portion of the cecum was ligated. The cecum was then punctured twice with a 21-gauge syringe needle, and a small amount of intestinal contents was extruded. The cecum was replaced, and the abdominal incision was closed with intermittent sutures. Preheated saline (37 °C, 50 ml/kg) was administered to aid resuscitation. 5-MTP (M4001, Sigma-Aldrich) was administered intraperitoneally or orally to the mice at 23.4 mg/kg for the required groups. The sham-operative group underwent the same procedure without cecal ligation or puncture.

Bacterial strain and fibrin clot preparation

Escherichia coli (Migula) Castellani and Chalmers strain (ATCC25922) was obtained from the BeNa Culture Collection and cultured in LB broth. The number of bacteria was estimated by measuring the optical density at A600 using a spectrophotometer. An aliquot of the culture medium was pelleted and resuspended with fibrinogen (1%) and thrombin (0.01 U) in PBS. Fibrin clots without bacteria were used as sham controls.

Bacterial load analysis

For quantitative assessment of bacterial load, biological samples including whole blood, peritoneal lavage fluid (PLF), and homogenized lung tissue were collected 24 h after CLP procedures. Serial dilutions of each sample type were prepared under sterile conditions, followed by inoculation of 100 uL aliquots onto nutrient agar plates and Columbia blood agar plates. Cultivation was performed in duplicate under controlled atmospheric conditions, using both aerobic and anaerobic environments maintained at 37 °C. After 24 h of incubation, CFUs were counted. Final bacterial loads were normalized to sample volume for liquid samples (expressed as CFU/mL) or tissue mass for organ samples (expressed as CFU/g).

In vivo imaging experiment

Mice were orally administered with bioluminescent *E. coli* (Lux-CDABE) for five consecutive days prior to surgery and were anesthetized 24 h post-operation for in vivo imaging. The AmiHTX imaging system was used to acquire and analyze photon emissions from regions of interest. The imaging parameters were set as follows: binning = 2, emission filter wavelength = open, exposure time = 15 s, field of view (FOV) = 25, *F*-stop = 1.2, object height = 1.5.

Antibiotic treatment and fecal microbiota transplantation

We administered an antibiotic (ABX) cocktail including vancomycin (100 mg/kg), neomycin sulfate (200 mg/kg), metronidazole (200 mg/kg), and ampicillin (200 mg/kg), all homogenized in phosphate-buffered saline (PBS), to 6–8-week-old male C57BL/6 mice. The ABXs were given intragastrically once a day for 3 days to deplete the gut microbiota [22]. For the fecal microbiota transplantation (FMT) experiment, fresh feces from either $Ace2^{-/y}$ or $Ace2^{+/y}$ littermate mice were collected and homogenized in PBS at a concentration of 100 mg/ml. The homogenate was centrifuged to pellet debris, and the supernatant, supplemented with an equal volume of 40% glycerol, was stored at −80 °C. Post-ABX treatment, wild-type (WT) C57BL/6 mice were randomly divided into two groups and received 200 µl of the fecal suspension by oral gavage daily for 5 days.

Measurement of intestinal permeability

Intestinal permeability was assessed by measuring the serum concentration of fluorescein isothiocyanate-dextran (FITC-dextran, 4 kDa, Sigma Aldrich).

Following the operation, mice were administered FD-4 solution orally at a dose of 20 mg/kg, 3 h before sacrifice. Blood samples were collected and centrifuged at 3000 rpm at 4 °C for 10 min to obtain serum. The fluorescence intensity of serum samples and serial dilutions of an FD-4 standard was measured on a SpectraMax M5 plate reader (Molecular Devices) at 485 nm excitation/528 nm emission. Serum FITC-dextran concentration was calculated using the standard curve as a reference.

Determination of lung wet/dry ratio

After the mice were sacrificed, the left lung lobes were absorbed with filter paper, weighed, and then the tissues were dried at 70 °C for 24 h. The dry weight was taken and the wet/dry ratios of the lungs were calculated.

16S rRNA gene sequencing

Total genomic DNA was extracted from fecal samples of eight littermate mice using the TGuide S96 Magnetic Soil/Stool DNA Kit (Tiangen Biotech, Beijing Co., Ltd.) following the manufacturer's instructions. The V1-V9 hypervariable regions of the 16S rRNA gene were amplified using specified primers (27 F: AGRGTT TGATYNTGGCTCAG; 1492R: TASGGHTACCTT GTTASGACTT). Polymerase chain reaction (PCR) products were then purified, quantified, and homogenized to prepare a sequencing library. Quality control of the library was performed before sequencing using the PacBio Sequel II system (Beijing Biomarker Technologies Co., Ltd.). Downstream data and the CCS file were exported by smrtlink analysis software, and sample-specific sequences were identified by barcode and converted into fastq format. Bioinformatics analysis was performed using BMKCloud.

Metabolomics

Metabolic profiling of feces from the same eight littermate mice was performed using a Waters Acquity I-Class PLUS UPLC tandem Waters Xevo G2-XS QTOF high-resolution mass spectrometer. Columns were purchased from Waters Acquity (UPLC HSS T3 column 1.8 μm 2.1 × 100 mm). Positive ion mode: mobile phase A: 0.1% formic acid aqueous solution; mobile phase B: 0.1% formic acid acetonitrile; negative ion mode: mobile phase A: 0.1% formic acid aqueous solution; mobile phase B: 0.1% formic acid acetonitrile; Injection volume 1 μL primary and secondary mass spectrometry data were collected by acquisition software (MassLynx V4.2, Waters). The low collision energy is 2 V, the high collision energy range is 10–40 V, and the scanning frequency is 0.2 s for a mass spectrum. The parameters of the electron spray ionization (ESI) ion source are as follows: capillary voltage: 2000 V (positive ion mode) or −1500 V (negative ion mode); cone voltage: 30 V; ion source temperature: 150 °C; desolvent gas temperature 500 °C; backflush gas flow rate: 50 L/h; desolventizing gas flow rate: 800 L/h. Raw data was processed by a Progenesis QI software for peak extraction, peak alignment, and other data processing operations, based on the Progenesis QI software online METLIN database and self-built library for identification. Principal component analysis and Spearman correlation analysis were used to judge the repeatability of the samples. *T*-test was used to calculate the difference significance *p*-value of each compound. The R language package ropls was used to perform OPLS-DA modeling. The VIP value of the model was calculated using multiple cross-validation. *P* value and the VIP value of the OPLS-DA model were adopted to screen the differential metabolites, applying a fold change > 1, *P* value < 0.05 and VIP > 1 criteria.

Quantification of 5-methoxytryptophan was performed by SHIMADZU Nexera UHPLC LC-30 A tandem AB Sciex 4000 Q-trap. The column was purchased from Waters, UPLC BEH Amide column (1.7 μm, 2.1 × 100 mm). Mobile phase A: 100% H_2O 25 mM CH3 $COONH_4$ + 25 mM NH_4OH, B-100% ACN. Elution gradient at 0.3 mL/min was applied as follows: 0 ~ 1 min, 85% B; 1 ~ 12 min, 65% B; 12 ~ 12.1 min, 40% B; 12.1 ~ 15 min, 40% B; 15 ~ 15.1 min, 85% B; 15.1 ~ 20 min, and 85% B. ESI ion source parameters are as follows, ion source temperature: 600 °C; capillary voltage: −4500 V (negative ion mode); backflush gas flow rate: 20 psi; GS1 and GS2: 60 psi. The most responsive parent-to-daughter ion transition (233.1/146.1) was selected to record the analytes in multiple reaction monitoring mode. Raw data was extracted and processed by SCIEX OS software as described above.

RNA sequencing

The total RNA of ileal tissues was extracted using Trizol reagent (AG21102, Accurate Biology) and quantified with a NanoDrop 2000 spectrophotometer (Thermo Fisher Scientific, Wilmington, DE). Sequencing libraries were generated from 1 μg of RNA using Hieff NGS Ultima Dual-mode mRNA Library Prep Kit for Illumina (Yeasen Biotechnology (Shanghai) Co., Ltd.) and sequenced on an Illumina NovaSeq platform to generate 150 bp paired-end reads. The raw reads were further processed with a bioinformatic pipeline tool (BMKCloud). Differential expression analysis was performed using the DESeq2, with *p* values adjusted using the Benjamini–Hochberg method. Genes with an adjusted *p* value < 0.05 and fold change ≥ 1.5 found by DESeq2 were assigned as differentially expressed. Gene Ontology (GO) enrichment analysis of the differentially expressed genes was implemented by the clusterProfiler package based on Wallenius non-central hyper-geometric distribution (Young et al., 2010).

For the Kyoto Encyclopedia of Genes and Genomes (KEGG) pathway enrichment analysis, we used the KOBAS (Mao et al., 2005) database and clusterProfiler software to test the statistical enrichment of differential expression genes. Raw data are available at the GEO database (accession number GSE267002).

Cell culture and treatments

Caco-2 cells were cultured in Dulbecco's modified Eagle medium (DMEM, C11995500BT, Gibco) supplemented with 10% fetal bovine serum (FBS, FSP500, ExCell), at 37 °C in a humidified atmosphere containing 5% CO_2. For the in vitro experiment, Caco-2 cells were seeded onto 6-well plates and cultured for 24 h with a complete medium. Thereafter, the cells were serum-starved overnight prior to drug treatments in a serum-free medium. Cells were preincubated with 100 μM 5-methoxy-DL-tryptophan (Sigma-Aldrich) for 30 min (for required groups). TNF-α (RP00001, Abclonal) was used at a concentration of 100 ng/ml, hydrogen peroxide was used at 100 μM.

Cell proliferation assay

The proliferation of cells was assessed in vivo by means of a 5-ethynyl-20-deoxyuridine (EdU) assay (40275ES60, YEASEN) and in vitro by a Cell Counting Kit-8 (CCK-8) (C0038, Beyotime) in accordance with the instructions provided by the manufacturer. Mice that underwent CLP and were treated with PBS or 5-MTP were administered with EdU by intraperitoneal injection at a dose of 5 mg/kg body weight 6 h before sacrifice. The intestinal segments were fixed, paraffin-embedded, sectioned, deparaffinized, and hydrated in accordance with the previously described methodology. The tissue sections were treated with 0.5% Triton X-100 (T8200, Solarbio) for 20 min and washed three times with 3% bovine serum albumin (BSA, BS114, Biosharp) in PBS. The tissue sections were incubated with the Click-iT reaction mixture for 30 min in the dark. The reaction was terminated by washing the sections in 3% BSA in PBS. The sections were then counterstained using Mounting Medium with 4',6-diamidino-2-phenylindole (DAPI, Ab104139, Abcam).

Cell cycle analysis

Caco-2 cells were seeded in a 6-well plate and maintained in DMEM supplemented with 10% FBS for 24 h at 37 °C. Following a 30-min preincubation with 5-MTP, the cells were exposed to TNF-α at a concentration of 100 μM for a period of 24 h. H_2O_2 was added at a concentration of 100 μM. The cells in the plate were harvested, washed, and resuspended in PBS and fixed with 4 °C precooled ethanol overnight. The following day, the cells were resuspended in 2 mL PBS for 15 min and washed twice. Subsequently, the cells were pelleted and resuspended in 1 mL of a DNA staining solution (propidium iodide, PI) for 30 min in a dark environment. The DNA content analysis was carried out using a CytoFLEX flow cytometer (BECKMAN COULTER) and the Flowjo v10.10.0 software (BD Biosciences).

Western blot

The total protein content of the tissue samples from mice or cells was extracted using a RIPA lysis buffer (P0013B, Beyotime) with the addition of a 1% protease inhibitor cocktail mix (KGP603, Keygen). After a centrifuging at 12,000 rpm, 4 °C for 15 min, the supernatant was collected and heated with 5× loading buffer (FD002, FdBio Science) at 95 °C for 7 min. The total protein concentration was then determined using the Pierce™ BCA Protein Assay Kit (23,225, Thermo Fisher). Equal amounts of each protein sample (20–40 μg) were loaded and separated in 7.5–12.5% SDS-PAGE gels by electrophoresis, transferred to PVDF membranes (ISEQ00010, Merck Millipore), and blocked for 1 h in 5% BSA or non-fat milk in Tris-buffered saline with Tween-20 (TBST). Subsequently, the blots were incubated with primary antibodies overnight at 4 °C, followed by washing in TBST and incubation with horseradish peroxidase (HRP)-labeled secondary antibodies for 1 h at room temperature. Finally, the signals were detected using an enzyme-linked enhanced chemiluminescence (ECL) reagent (BL520 A, Biosharp) and quantified by using ImageJ software. The antibodies used are listed in Table 1.

Real-time quantitative polymerase chain reaction

Total RNA was extracted from tissue or cells using the AG RNAex Pro Reagent (AG21102, Accurate Biology) and isopropyl alcohol (I112011, aladin), and its purity and concentration were determined by a Nanodrop 2000 (Thermo Fisher Scientific). Single-strand cDNA was generated using the HiScript II QRT SuperMix for quantitative PCR (qPCR) (R223-01, Vazyme) in accordance with the manufacturer's instructions. Quantitative real-time PCR (qRT-PCR) was performed using Taq Pro Universal SYBR qPCR Master Mix (Q712-02, Vazyme). The fold changes in the expression levels of the targets were calculated using the $2^{-\Delta\Delta CT}$ method with β-actin as an endogenous reference. The primers used in the qRT-PCR were designed with NCBI Primer-BLAST or acquired from Primer-bank (Table 2).

Histology staining, immunohistochemistry, and immunofluorescence

Tissues from mice were isolated and fixed in a 4% paraformaldehyde solution for 24 h at room temperature. They were then embedded in paraffin to obtain tissue

Table 1 Antibodies

Product title	Source	Identifier
Anti-ZO1 Polyclonal antibody	Thermo Fisher Scientific	61–7300
Anti-Occludin Monoclonal Antibody	Thermo Fisher Scientific	33–1500
Anti-Occludin Polyclonal Antibody	Proteintech	27,260–1-AP
CDC25B Monoclonal antibody	Proteintech	10,009,433
Myeloperoxidase (MPO) Rabbit pAb	ABclonal Technology	5,500,017,439
Phospho-WEE1 (Ser642) Antibody	ABclonal Technology	10,151,170
Phospho-CDK1-Y15 Rabbit pAb	ABclonal Technology	5,500,028,738
CDK1 Rabbit pAb	ABclonal Technology	0081150201
Cyclin B1 Rabbit pAb	ABclonal Technology	5,500,008,677
Phospho-AKT1-S473 Rabbit pAb	ABclonal Technology	5,500,020,007
Phospho-PI3 KP85α/γ/β-Y467/Y199/Y464 Rabbit pAb	ABclonal Technology	5,500,028,946
PI3 Kinase p85 alpha/beta Rabbit mAb	ABclonal Technology	A22487
TPH1 Rabbit pAb	ABclonal Technology	0205950101
Ki67 Rabbit mAb	ABclonal Technology	4,000,122,207
β-Actin Rabbit mAb	ABclonal Technology	9,100,026,001
Akt(pan)(11E7) Rabbit monocloning antibody	Cell Signaling Technology	4685 s
PCNA Rabbit pAb	BOSTER Biological Technology	BM0104
Anti-PCNA antibody [PC10]	Abcam	ab29
GAPDH Monoclonal antibody	Proteintech	60,004–1-Ig
ACE2 polyclonal antibody	Proteintech	21,115–1-AP
HRP-conjugated Affinipure Goat Anti-Mouse IgG(H + L)	Proteintech	SA00001-1
HRP-conjugated Affinipure Goat Anti-Rabbit IgG(H + L)	EarthOx	E030120

sections. The sections were deparaffinized by xylene and hydrated. Pathological damage in different organs was assessed by conducting hematoxylin and eosin (H&E), periodic acid Schiff staining (PAS), and alcian blue periodic acid Schiff (AB-PAS) staining (BH0022, ERFUL BIOLOGY). Semiquantitative histological scores of lung injury included the thickness of alveolar walls, alveolar fusion, hemorrhage in the air compartment, inflammation, and tissue exudation. To analyze the distribution and expression of specific proteins, the sections were subjected to an epitope retrieval process. This involved steaming in sodium citrate buffer pH 7.0 (AR0024, BOSTER), treating the sections with 10% goat serum (ZLI-9021, ZSGB-BIO) and 3% H_2O_2 to avoid non-specific binding, and incubating them with primary antibodies overnight at 4 °C. Following three times of washing with PBS and trisodium citrate buffer (AR0024, BOSTER), the sections were incubated with the corresponding secondary antibodies for 1 h at room temperature. For histology staining, immunohistochemistry (IHC), the DAB Kit (ZLI-9018, ZSGB-BIO) was used to visualize the staining, whereas hematoxylin was employed as a counterstain. In immunofluorescence (IF), a mounting medium with DAPI was used to counterstain.

Statistical analysis

The data presented in this study are expressed as mean ± standard error (X ± SD). Data were analyzed and plotted using R software with IDE R Studio and GraphPad Prism software (9.5.0). Survival analysis was performed by Mantel-Cox log-rank test. For statistical analysis between two groups, data conforming to a normal distribution and homogeneity of variance were analyzed by a two-tailed *t*-test. For groups with non-normal distribution, Mann–Whitney U test was used. For mean analysis between three groups or more, one-way ANOVA and Sidak's post hoc analysis were employed. A value of $P < 0.05$ was considered significant.

Results

Leaky gut exacerbates sepsis and is highly positively correlated with shed ACE2 levels in sepsis

From 2020 to 2024, 71 septic patients who met the inclusion criteria were enrolled. Baseline patient characteristics are summarized in Additional file 1. Serum levels of ACE2 as well as LPS binding protein (LBP) (an indicator of gut leak) were significantly higher in patients than in healthy volunteers (Fig. 1A, B). Furthermore, a positive correlation was observed between both parameters and the SOFA index (Fig. S1 A, B). To confirm the upregulated serum ACE2 level in sepsis, we performed a

Table 2 Primers

Gene symbol	Sequence	Gene symbol	Sequence
H-TJP1-F	ACCAGTAAGTCGTCCTGATCC	Tlr2-R	AGGCGTCTCCCTCTATTGTATT
H-TJP1-R	TCGGCCAAATCTTCTCACTCC	Tlr4-F	ATGGCATGGCTTACACCACC
H-OCLN-F	ACAAGCGGTTTTATCCAGAGTC	Tlr4-R	GAGGCCAATTTTGTCTCCACA
H-OCLN-R	GTCATCCACAGGCGAAGTTAAT	Tjp1-F	GCTTTAGCGAACAGAAGGAGC
H-IL1B-F	ATGATGGCTTATTACAGTGGCAA	Tjp1-R	TTCATTTTTCCGAGACTTCACCA
H-IL1B-R	GTCGGAGATTCGTAGCTGGA	Actb-F	GTGACGTTGACATCCGTAAAGA
H-IL6-F	ACTCACCTCTTCAGAACGAATTG	Actb-R	GCCGGACTCATCGTACTCC
H-IL6-R	CCATCTTTGGAAGGTTCAGGTTG	Ocln-F	TGAAAGTCCACCTCCTTACAGA
H-TNF-F	CCTCTCTCTAATCAGCCCTCTG	Ocln-R	CCGGATAAAAAGAGTACGCTGG
H-TNF-R	GAGGACCTGGGAGTAGATGAG	Pik3r1-F	CATAACCTGCAAACACTGCCC
H-ACE2-1 F	CGAAGCCGAAGACCTGTTCTA	Pik3r1-R	ATCCTGCAAGGACATATTGTTGT
H-ACE2-1R	GGGCAAGTGTGGACTGTTCC	Pik3ca-F	CACTCGTCACCATCAAACATGA
H-CCL2-F	CAAGCAGAAGTGGGTTCAGGATT	Pik3ca-R	AGGGTTGAAAAAGCCGAAGGT
H-CCL2-R	TCTTGGGTTGTGGAGTGAGTGTTC	Akt1-F	ATGAACGACGTAGCCATTGTG
H-CXCL2-F	CGCCCATGGTTAAGAAAATCA	Akt1-R	TTGTAGCCAATAAAGGTGCCAT
H-CXCL2-R	CCTTCTGGTCAGTTGGATTTGC	Ccnb1-F	CTTGCAGTGAGTGACGTAGAC
H-CDK1-F	AAACTACAGGTCAAGTGGTAGCC	Ccnb1-R	CCAGTTGTCGGAGATAAGCATAG
H-CDK1-R	TCCTGCATAAGCACATCCTGA	Ccnb2-F	GCCAAGAGCCATGTGACTATC
H-CCNB1-F	TTGGGGACATTGGTAACAAAGTC	Ccnb2-R	CAGAGCTGGTACTTTGGTGTTC
H-CCNB1-R	ATAGGCTCAGGCGAAAGTTTTT	Ccna1-F	CAGTTTCCCCAATGCTGGTTG
H-CDC25 A-F	GTGAAGGCGCTATTTGGCG	Ccna1-R	CCTCTGCATACTCCGTTACGTTA
H-CDC25 A-R	TGGTTGCTCATAATCACTGCC	Ccna2-F	GTCCTAACGCTCCCATCTCC
H-CDC25B-F	ACGCACCTATCCCTGTCTC	Ccna2-R	TCGGAAAGAGTGTCAGCCTC
H-CDC25B-R	CTGGAAGCGTCTGATGGCAA	Cdk1-F	AGAAGGTACTTACGGTGTGGT
H-CDC25 C-F	TCTACGGAACTCTTCTCATCCAC	Cdk1-R	GAGAGATTTCCCGAATTGCAGT
H-CDC25 C-R	TCCAGGAGCAGGTTTAACATTTT	cdc25a-F	TCCCTGACGAGAATAAATTCCCT
H-ACTB-F	CATGTACGTTGCTATCCAGGC	cdc25a-R	TCGATGAGGTGAAAGGTGTCG
H-ACTB-R	CTCCTTAATGTCACGCACGAT	cdc25b-F	TCCGATCCTTACCAGTGAGG
Ace2-F	GGCGACAAGCACAGACTACAA	cdc25b-R	GGGCAGAGCTGGAATGAGG
Ace2-R	GCCATCTCGTTTTTCAGGACC	cdc25c-F	GTTTCAGCACCCAGTTTTAGGT
Tlr2-F	GCAAACGCTGTTCTGCTCAG	cdc25c-R	AGAATGCTTAGGTTTGCCGAG

polymicrobial sepsis model on WT C57BL/6 mice. Compared with sham-operated mice, septic mice exhibited more than two-fold ACE2 concentration (Fig. 1C). Furthermore, a temporal gradient measurement of serum ACE2 demonstrated that ACE2 shedding occurred 1-h post-operation and continued to rise (Fig. S1 C). Given that ACE2 is a transmembrane protein, we sought to identify the primary source of soluble ACE2, which is cleaved into the circulation. It has been reported that the small intestine has the highest reads per kilobase

(See figure on next page.)

Fig. 1 Leaky gut exacerbates sepsis and is highly positively correlated with shed ACE2 levels in sepsis. **A** Serum ACE2 levels of healthy volunteers and septic patients (*n* (healthy volunteer) = 18, *n* (septic patient) = 71). **B** Serum LPS-binding protein (LBP) levels of healthy volunteers and septic patients (*n* (healthy volunteer) = 16, *n* (septic patient) = 71). **C** Serum ACE2 levels in sham and CLP (cecal ligation and puncture) mice (*n*(sham) = 7, *n*(CLP) = 17). **D**, **E** ACE2 protein levels of the lung, small intestine, colon, liver, gallbladder, and kidney by Western blot (*n* = 4). **F**–**J** ACE2 protein levels of the small intestine, kidney, and lung and ADAM17 protein levels of the small intestine (*n* = 6). **K** Feces ACE2 levels of sham and CLP mice (*n* = 6). **L** Immunohistochemistry (IHC) staining of ACE2 in the ileum (scale bar = 50 μm). **M** IL-6, Pro-BNP, lactic acid, LBP, urea, age, WBC, PO_2/FiO_2 ratio, IBIL, and PCT levels were shown between survivors and non-survivors by fold change. **N** The receiver operating characteristic (ROC) curve of LBP for predicting in-hospital death of patients with sepsis (*n* = 71). **O** Correlation analysis between LBP, ACE2, and clinical tests (*n* = 71). Data are presented as mean ± SD by the Student's *t* test. ns = no significance, **p* < 0.05, ***p* < 0.01, ****p* < 0.001, and **** *p* < 0.0001. Abbreviations: IL-6, interleukin-6; pro-BNP, pro-brain natriuretic peptide; Lac, lactic acid; LBP, lipopolysaccharide-binding protein; WBC, white blood cell count; IBIL, indirect bilirubin; PCT, procalcitonin

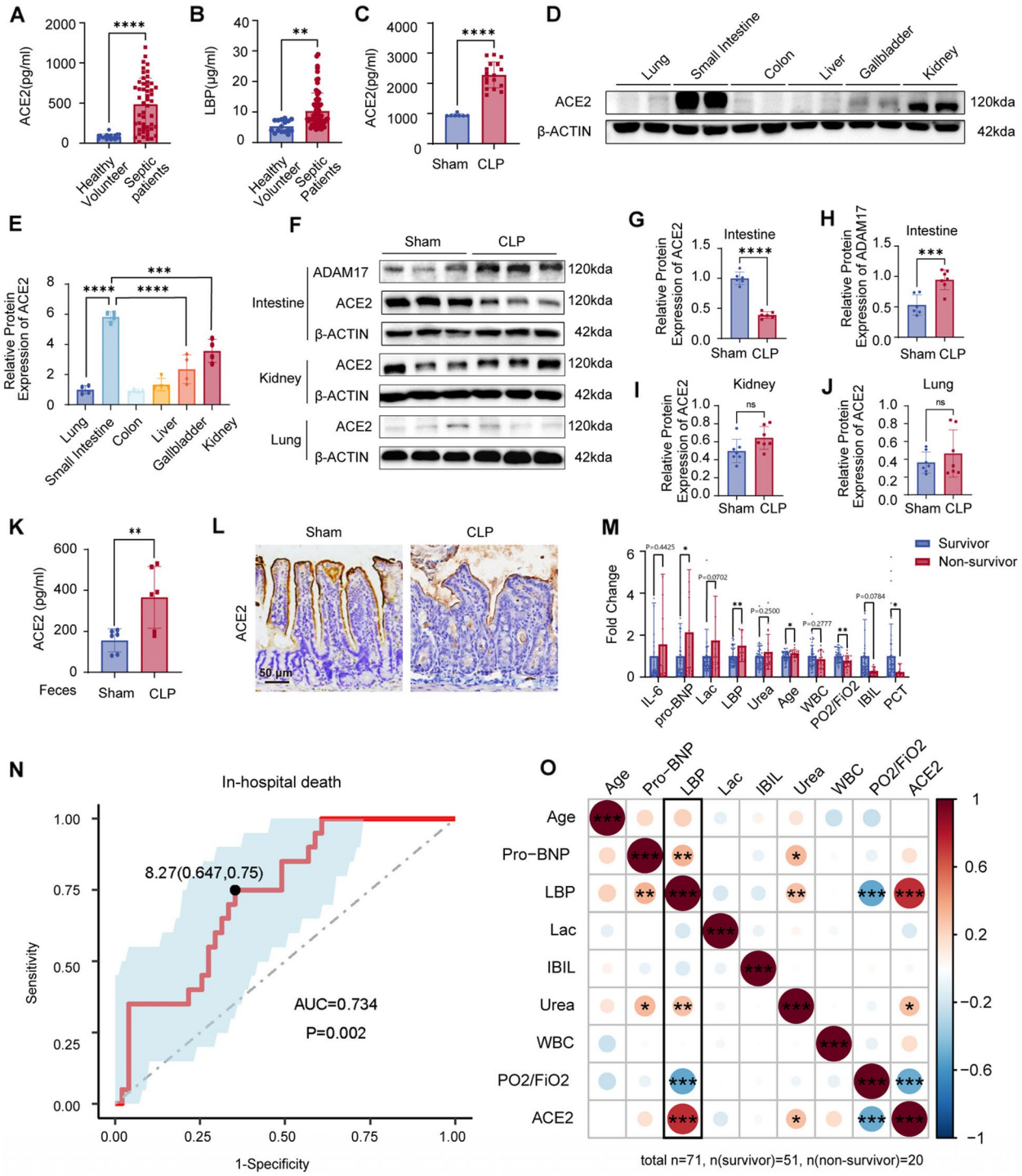

Fig. 1 (See legend on previous page.)

per million mapped reads (RPKM) in tissues [23]. We verified that the ACE2 protein level in the small intestine also exceeded that of other major tissues, including the lung, colon, liver, gallbladder, and kidney (Fig. 1D-E) and that it dropped in septic mice. Concurrently, intestinal ADAM17 sheddase and fecal ACE2 levels were increased, suggesting a cleavage on the luminal side. Notably, ACE2 levels remained constant in the kidneys (which exhibited the second-highest ACE2 expression) and lungs in sepsis (Fig. 1F-L). These findings indicate that the small intestine is probably a major source of ACE2 shedding.

When patients were grouped according to clinical outcome into survivors and non-survivors, pro-BNP, lactic acid, age, and LBP levels were elevated, whereas PO_2/FiO_2, IBIL, and PCT levels were lower in non-survivors during sepsis (Fig. 1M). Receiver operating characteristic (ROC) curve analysis showed that LBP could predict in-hospital death with an area under the curve (AUC) of 0.734 (Fig. 1N). Whilst serum ACE2 levels were found to be elevated in cases of sepsis, the concentrations observed were comparable between survivors and non-survivors (Fig. S1D). Consequently, the levels of this marker were inadequate to predict in-hospital death (Fig. S1E). We then analyzed the possible correlations between ACE2, LBP, and clinical test results (Fig. 1O). Serum LBP was positively correlated with pro-BNP ($r = 0.346$, $p = 0.004$), urea ($r = 0.300$, $p = 0.009$), and ACE2 levels ($r = 0.737$, $p < 0.001$) and negatively correlated with PO_2/FiO_2 ($r = -0.517$, $p < 0.001$). These results suggest that gut leak may accelerate the progress of sepsis and that ACE2 might play a role in maintaining gut barrier integrity.

ACE2 contributes to gut integrity in septic mice

To ascertain the role of membrane form of ACE2 (m-ACE2) during sepsis, we employed the *Ace2*$^{-/y}$ (KO) mice and conducted a sham or CLP operation together with a C57BL/6 WT control (Fig. 2A). We used agarose gel electrophoresis for mouse genotyping and validated the knockout efficiency in the ileum (Fig. S1 F, G). The cecal ligation and puncture model was produced as described previously. The overall effect of ACE2 on mice was first investigated using survival analysis (Fig. 2B). The sham operation did not affect the survival rate in both groups. The CLP mice began to show clinical syndromes 6 h post-operation, featuring less movement, ruffled hair, and diarrhea. The WT-CLP and KO-CLP group mice exhibited acute mortality. However, while the survival curve of the WT-CLP group reached a plateau between 12- and 24-h post-operation, the survival rate of the KO-CLP group continued to decline. (n (WT-CLP) = 15, 7-day survival rate 52%, 95% CI 21.9–60.7%; n (KO-CLP) = 15, 7-day survival rate 20.0%, 95% CI 19.9–60.0%; $P = 0.0012$). KO-CLP mice exhibited more body weight loss (Fig. S1H), higher levels of inflammatory cytokine TNF, serological infectious parameter procalcitonin (PCT), and lower glucose levels in comparison with WT-CLP mice (Fig. 2C–E). The worsened survival rate of KO mice suggests that ACE2 may be beneficial in overcoming septic shock. As ACE2 was rather specific and highly enriched on the luminal side of the villi (Fig. S1G), we considered whether the loss of ACE2 might compromise the functions of the intestinal epithelial cells, which act as the first line of defense against potentially pathogenic microorganisms. The integrity of the intestinal epithelium was assessed by measuring the intensity of FITC-dextran (MW 4 kDa) fluorescence in serum [24]. The FITC intensity was found to be significantly higher in the WT-CLP group than in its sham control, indicating the presence of gut leak in sepsis. Interestingly, the knockout of *Ace2* did not influence the permeability of epithelial cells in the sham-operated group, whereas it disrupted epithelial integrity severely in sepsis (Fig. 2F). In evaluations of the epithelial mechanical barrier, it was confirmed that CLP-operated mice exhibited villi damage and discontinuities. Structure shattering and stripping were more severe in KO mice. The intestinal chemical barrier was evaluated using AB-PAS staining (Fig. 2G middle panel). The knockout of *Ace2*, as well as CLP operations on WT mice, led to a mild loss of goblet cells. In contrast, KO mice exhibited aggravated goblet cell damage and lost the majority of their goblet cells. Tight junction (TJ) proteins were evaluated by immunofluorescence (IF) and Western blot (Fig. 2G lower panel, Fig. 2H-K). Intestinal ZO-1 or OCLN levels were unchanged in sham animals, while they were reduced in sepsis. Similarly, these TJ protein levels were even lower in KO mice. To rescue the loss of ACE2, hACE2$^{+/+}$ (OE) mice (ICR background) were employed. Mice were genotyped and the overexpression was confirmed in the ileum (Fig. S1I, J). Levels of shed ACE2 were found to be elevated in the feces and serum of OE mice, and they increased following CLP surgery (Fig. S1 K, L). OE-CLP mice exhibited improved survival rates, less loss of body weight, higher glycemia levels, and lower inflammatory markers (Fig. S1M-Q). Serum FITC intensity was reduced in OE-CLP mice compared with WT-CLP mice (Fig. S1R). Intestinal TJ protein ZO-1 and OCLN were also partly rescued in OE-CLP mice (Fig. S1S). Furthermore, HE and AB-PAS staining revealed that intestinal epithelial barrier and goblet cell damage were less severe (Fig. S1 T, U). In brief, upon sepsis challenge, loss of ACE2 exacerbates intestinal barrier dysfunction and leads to a worse prognosis, which could be improved by overexpression of ACE2. However, merely knockout or overexpression of ACE2 barely affected intestinal barrier function and was asymptomatic. These results suggest an intriguing role ACE2 plays in maintaining gut homeostasis.

ACE2 reduces bacteria translocation and alleviates organ dysfunction in sepsis

Following gastric gavage of bioluminescent *E. coli*, bacterial luminal-basolateral translocation was assessed via the AmiHTX Imaging System 24 h post-operation. Bioluminescent *E. coli* was colonized in the recipients' gut upon a 5-day gavage. Bioluminescent imaging demonstrated that photon intensity was relatively low in the sham-operated groups. Given that gut homeostasis was maintained in

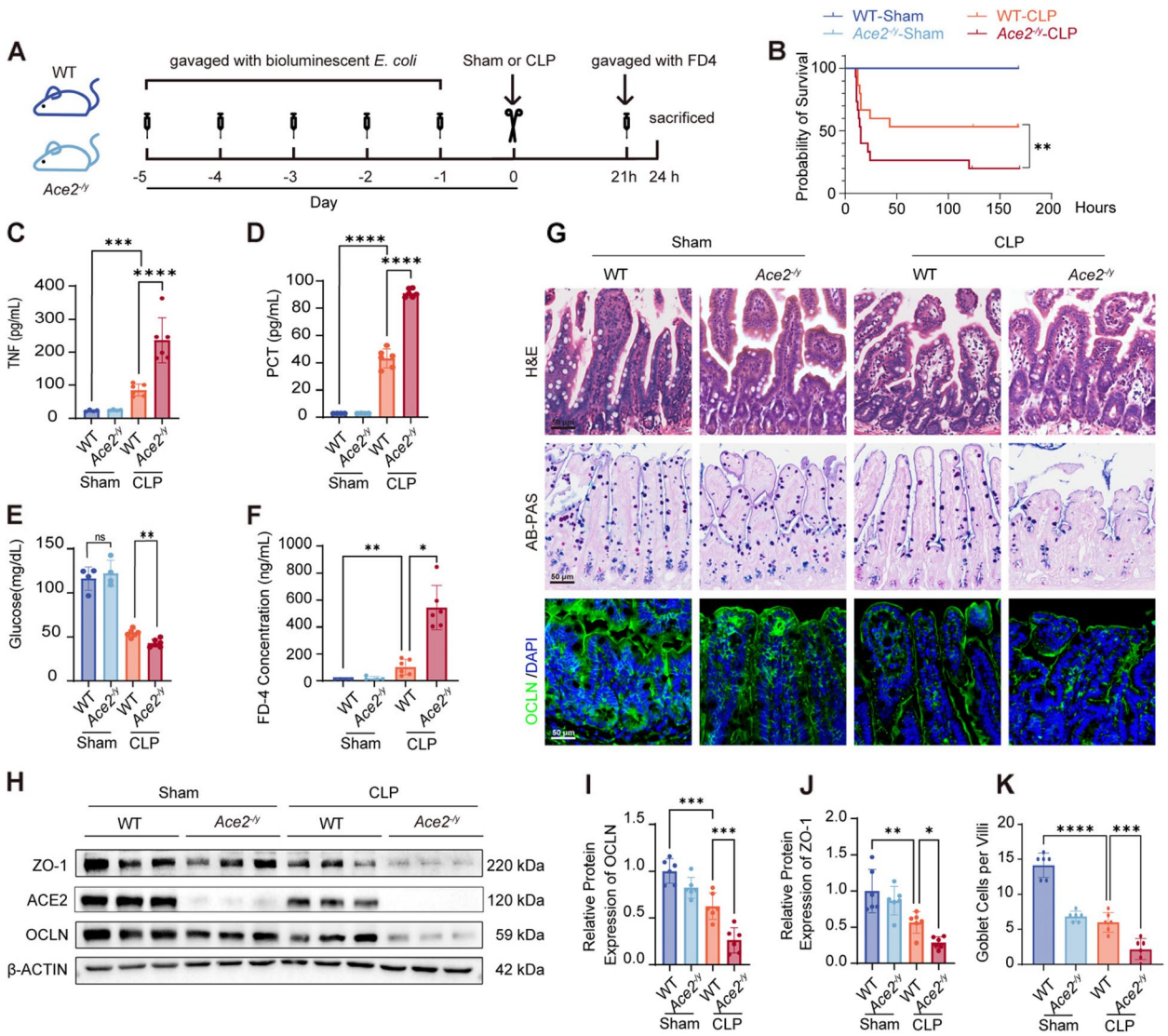

Fig. 2 ACE2 contributes to gut integrity in septic mice. **A** A schematic diagram of the experimental procedures. **B** Survival rates of Sham or CLP operation of both WT mice and *Ace2*$^{-/y}$ mice (n(Sham) = 5, n(CLP) = 15). **C**–**E** Serum TNF, PCT, and glucose concentration of WT mice and *Ace2*$^{-/y}$ mice underwent Sham or CLP operation (n = 4–15). **F** Fluorescein isothiocyanate-dextran (FITC-dextran; FD-4) was gavaged 3 h before sacrifice (20 mg/kg), and serum FD-4 concentration was examined (n = 4–15). **G** Hematoxylin and eosin (H&E) staining (upper panel), alcian blue periodic acid Schiff (AB-PAS) staining (middle panel), and IF staining of tight junction (TJ) protein OCLN (lower panel) in the ileum (scale bar = 50 μm). **H**–**J** Ileal ZO-1, OCLN, and ACE2 levels by Western blot (n = 6). **K** Quantification of goblet cells (n = 6). Data are presented as mean ± SD. ns = no significance, *p < 0.05, **p < 0.01, ***p < 0.001, and ****p < 0.0001 by two-tailed Student's t test, Mann–Whitney test, or one-way ANOVA and Sidak's post hoc analysis. Intergroup survival differences were analyzed by a log-rank test. Abbreviations: CLP, cecal ligation and puncture; TNF, tumor necrosis factor; PCT, procalcitonin; FD-4, fluorescein isothiocyanate-dextran; OCLN, occludin; ZO-1, zona occludens 1

both groups, the engineered *E. coli* was likely at a disadvantage in the competition with indigenous microbiota. For septic mice, significant photon signals were observed at the abdomen and chest area, indicating microbial dysbiosis in the gut and bacteria translocation to extra-intestinal organs in sepsis (Fig. 3A–C). The knockout of *Ace2* resulted in a more severe gut leak, while OE mice partly preserved the integrity of the epithelial barrier (Fig. S2 A-C). As the swift clearance of bacteria could reflect a defense strategy and predict the outcomes of sepsis [25, 26], bacterial counts of both aerobic and anaerobic bacteria (24 h after CLP) were analyzed in the blood, peritoneal lavage fluid (PLF), and lung samples (Fig. 3D, E). The knockout of *Ace2* resulted in a higher bacteria count. Excessive bacteria load in vital organs could disrupt oxidative and inflammatory balance during sepsis [27]. The

histological examination and wet/dry ratio of the lung tissues revealed the presence of acute lung injury in the CLP groups, characterized by inflammation, edema, alveolar septal thickening, and hemorrhage (Fig. 3F, G). In the kidney, the glomerular and tubular structures of the sham group remained intact. Following CLP, renal damage was observed, including swelling of the tubule epithelium, brush border abscission, tubular dilation, and elevation of serum creatinine levels (Fig. 3H, I). The knockout of *Ace2* led to a greater incidence of lung injury and renal dysfunction. Conversely, OE mice exhibited a mitigating effect on these organ dysfunctions (Fig. S2D-G). In addition to the polymicrobial sepsis model, we performed live-bacteria-induced sepsis in mice by implanting a fibrin clot containing *Escherichia coli* (*E. coli*) in the peritoneal cavity [28]. One million colony-forming units (CFU) were chosen for the experiments, as this dosage demonstrated a moderate 50% mortality within a 48-h period (Fig. S2H). Similarly, KO- *E. coli* mice exhibited worse survival rates, more weight loss, lower serum glucose levels, and higher TNF levels (Fig. S2I-L). Furthermore, villi damage and discontinuities were more severe in this group of mice (Fig. S2M, N), which led to more bacterial translocation (Fig. S3 A, B) and organ dysfunction (Fig. S3 C-F). These results suggest that KO mice were more susceptible to infectious challenges and that their intestinal barrier integrity was more easily compromised.

5-MTP was highly correlated with a reduced abundance of tryptophan-metabolizing bacteria in ACE2 knockout mice

Since *Ace2* knockout itself was not sufficient to induce observable intestinal leakage, potential mediators in the regulation of intestinal homeostasis were investigated. It is well established that the gut microbiota, as well as microbial metabolites, affect intestinal homeostasis. Furthermore, ACE2 has been reported to alter the microbial community [12]. However, a detailed profile of the gut microbiota in the absence of ACE2 was not available. As knockout of *Ace2* did not directly alter the expression of TJ proteins, we postulated that a pre-existing change, such as the loss of beneficial commensal bacteria or microbial metabolites, rendered the gut barrier of KO mice more susceptible to sepsis-induced gut leak. To taxonomically characterize the gut microbiota composition, 16S rRNA gene sequencing of intestinal contents was performed. The rarefaction curves and rank abundance curves demonstrated that the differences within the groups are small and that these samples were sufficient to depict the microbiome of both strains (Fig. S4 A, B). Knockout of *Ace2* significantly reduced the abundance of *verrucomicrobiae*, accompanied by an increase in *bacteroidia* and *clostridia* (Fig. S4 C, D). The Shannon indices were elevated in the KO mice compared to their WT littermates (Fig. 4A), indicating an increased microbial complexity at the operational taxonomic unit (OTU) level. The principal coordinate analysis (PCoA) and stacked bar chart separated the KO mice from their littermates (Fig. 4B–D). To identify significant bacterial taxa in the two groups, we employed the linear discriminant analysis effect size (LEfSe) method, which identified significant differences in the bacterial taxa with an LDA score of ≥ 4.5. *Akkermansia muciniphil* (s), *Verrucomicrobiales* (o), *Akkermansiaceae* (f), *Verrucomicrobiota* (p), *Akkermansia* (g), *Verrucomicrobiae* (c), and *uncultured_Barnesiella_sp.* (g) were found to be significantly less abundant in KO mice than in WT mice, while *Clostridia* (c), *Lachnospirales* (o), *Lachnospiracae* (f), and *Lachnospiraceae_NK4 A136_group* (g) were found to be more abundant in KO mice (Fig. 4E). In parallel, untargeted metabolomics was employed to generate a comprehensive picture of the metabolome of the two strains. A total of 1667 metabolites were identified, with 88 being upregulated and 293 being downregulated as a consequence of *Ace2* knockout (Fig. 4F). Samples were also separated into two distinct groups by PCoA (Fig. 4G). Volcano plots of the -log10 (*P*-value) as a function of log2(FC) were employed to visualize the significant changes in metabolites (Fig. 4H). The top five ranked metabolites that were downregulated in KO mice were 3'-hydroxyamobarbital, 2-cis-abscisate, demethyllactenocin, biopterin, and 5-methoxytryptophan (5-MTP). The top 5 upregulated metabolites were Mpomeovt, gamma-aminobutyryllysine, PG(LTE4/i-12:0), avenoleic acid, and N-nervonyl threonine. Among these

(See figure on next page.)

Fig. 3 ACE2 reduces bacteria translocation and alleviates organ dysfunction in sepsis. **A**–**C** In vivo imaging and photon quantifications of bioluminescent *E. coli* ($n = 3$). **D**, **E** Quantification of bacterial load in blood, peritoneal lavage fluid (PLF), and lung samples from mice who underwent sham or CLP operation ($n = 3$). **F** H&E staining and histopathological evaluation of the lungs (scale bar = 50 μm, $n = 5$). **G** Wet/dry ratio of the lungs ($n = 6$). **H** Periodic acid Schiff (PAS) staining and the histopathological evaluation of the kidneys. Tubular structural disruption was assessed with a semi-quantitative scale (0: no lesion; 1: < 20%; 2: 20–40%; 3: 40–60%; 4: 60–80%; 5: 80–100% (scale bar = 50 μm, $n = 4$–6). **I** Serum creatinine levels of the mice ($n = 6$). Data are presented as the mean ± SD. ns = no significance, *$p < 0.05$, **$p < 0.01$, ***$p < 0.001$, and ****$p < 0.0001$ by one-way ANOVA and Sidak's post hoc analysis. Abbreviations: PLF, peritoneal lavage fluid; Scr, serum creatinine

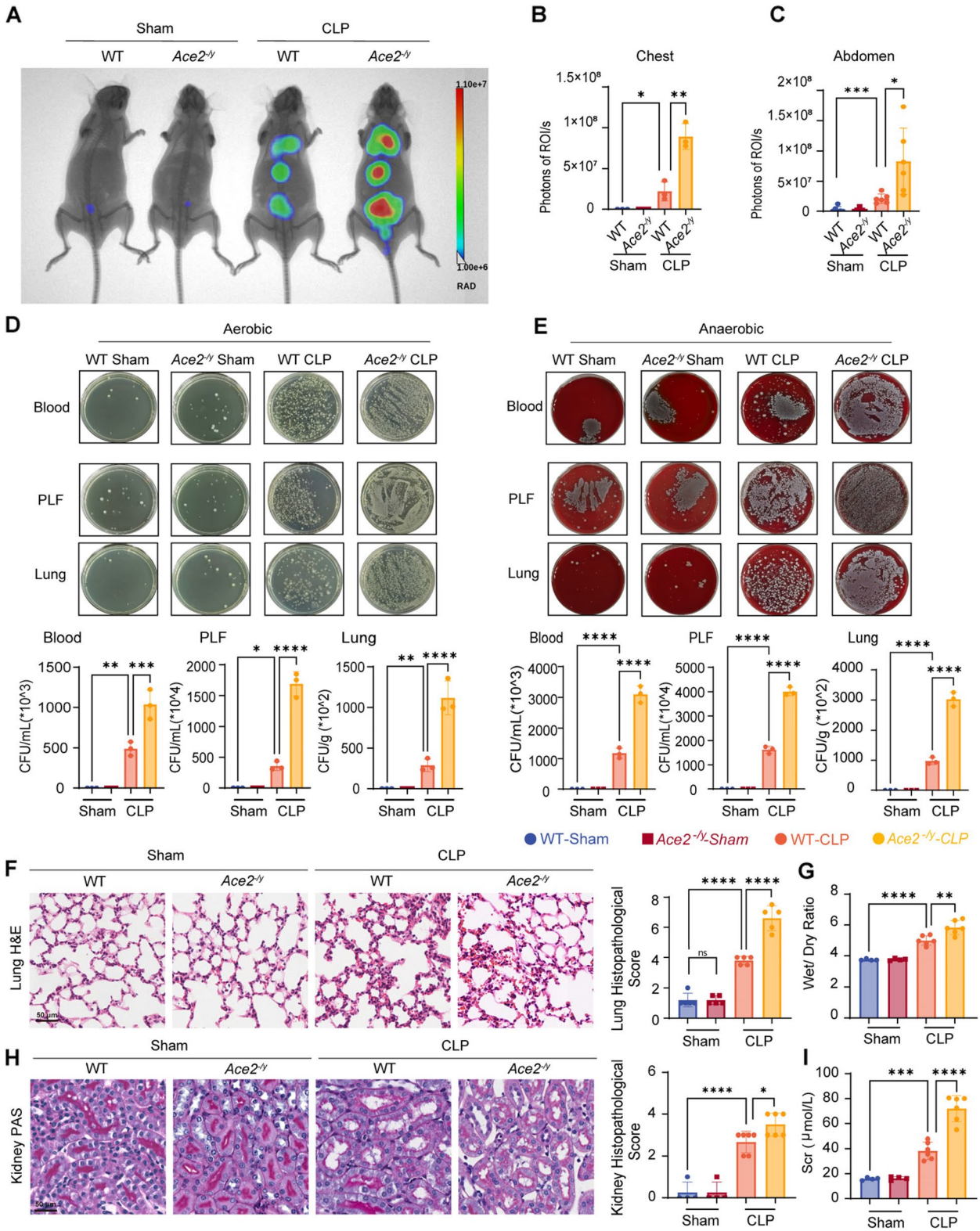

Fig. 3 (See legend on previous page.)

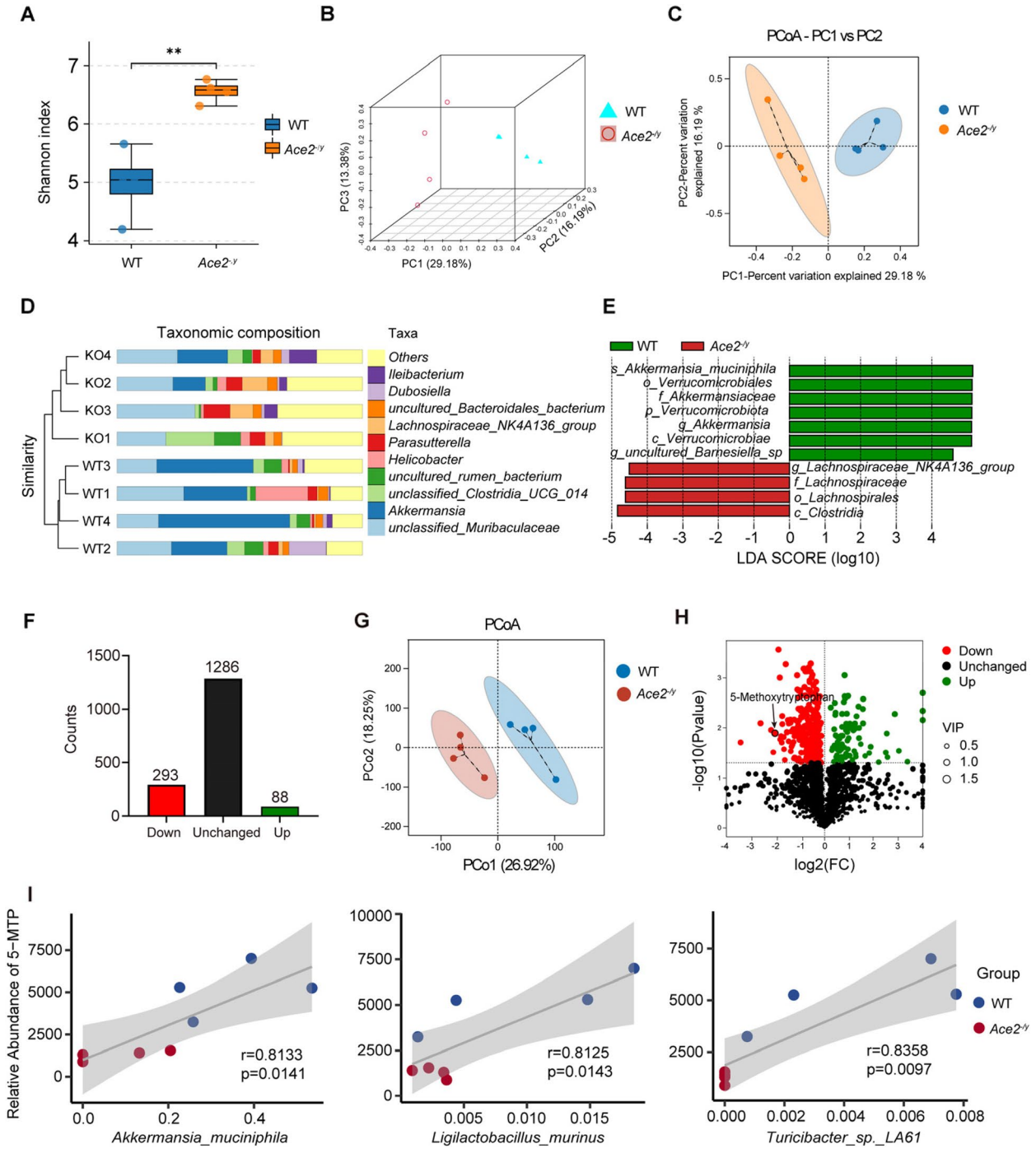

Fig. 4 Microbial composition and metabolites undergo alterations in *Ace2*$^{-/y}$ mice. **A** Shannon index of *Ace2*$^{-/y}$ mice and WT littermates ($n = 4$). **B**–**E** Beta-diversity analyzed by 3D principal component analysis (PCA), principal coordinate analysis (PCoA), cluster tree barplot, and Lefse analysis (LDA score > = 4.5) of WT and *Ace2*$^{-/y}$ mice. **F** Regulated metabolites detected by untargeted metabolomics ($n = 4$). **G** PCoA plot (PCo1 vs. PCo2) of metabolite composition in *Ace2*$^{-/y}$ mice and WT littermates ($n = 4$). **H** Volcano plot representation of regulated metabolite (black arrow indicating 5-methoxytryptophan). **I** Bacterial species highly correlate with 5-methoxytryptophan (5-MTP) abundance ($n = 8$). Data are presented as the mean ± SD. Alpha-diversity was calculated by two-tailed Student's *t* test, $^{**}p < 0.01$, and beta-diversity was calculated by the binary Jaccard method. Abbreviation: 5-MTP, 5-methoxytryptophan

metabolites, 5-MTP, a tryptophan derivative, was considered to be of greater biological significance. It has been reported that tryptophan hydroxylase 1 (TPH-1) is a key enzyme in the synthesis of 5-MTP [18]. However, the protein levels of instestinal TPH-1 were comparable between KO and WT mice (Fig. S4E, F). Altered levels of some other tryptophan metabolites may also indicate the aberrant tryptophan metabolism in KO mice (Fig. S4G, H). Tryptamine was reduced in KO mice while the level of its precursor, indole, had a tendency to increase ($p = 0.06$). Furthermore, correlation analysis was employed to characterize bacteria species associated with the 5-MTP alteration. A total of six species demonstrated a high correlation ($r > 0.8$) with 5-MTP. The *Akkermansia muciniphila* exhibited a correlation of 0.8133 with 5-MTP, with a 95% confidence interval of [0.2543, 0.9649] and a *p*-value of 0.0141. Similarly, the *Ligilactobacillus murinus* demonstrated a correlation of 0.8125 with 5-MTP, with a 95% confidence interval of [0.2522 to 0.9648] and a *p*-value of 0.0143. *Turicibacter sp. LA61* ($r = 0.8751$, 95%CI [0.4447 to 0.9772], $p = 0.0044$), *Adlercreutzia muris* ($r = 0.8557$, 95%CI [0.3804, 0.9734], $p = 0.0067$), *Romboutsia ilealis* ($r = 0.8358$, 95%CI [0.3190 to 0.9695], $p = 0.0097$), and *uncultured Barnesiella sp.* ($r = 0.8586$, 95%CI [0.3897 to 0.9740], $p = 0.0063$) were also identified as significant (Fig. 4I, Fig. S4I-K).

It is noteworthy that *Akkermansia muciniphila* outnumbered the other bacteria by 1055-fold (*Adlercreutzia muris*), 36-fold (*Ligilactobacillus murinus*), 167-fold (*Romboutsia ilealis*), 80-fold (*Turicibacter* sp. LA61), and 526-fold (*uncultured Barnesiella* sp.), suggesting the role between *Akkermansia muciniphila* and 5-MTP level could be dominant compared to other bacteria species (Fig. S4L).

The worsening of sepsis-induced gut leak is transferrable by fecal transplantation partially via 5-MTP

To figure out the role of the gut microbiota and microbial metabolites in sepsis, an antibiotic cocktail was administered to both mouse strains prior to the CLP operation. ABX depletion resulted in a deterioration of intestinal permeability in WT-CLP mice (Fig. S5 A-E). This was accompanied by TNF upregulation, hypoglycemia, weight loss, increased bacterial load, and a more severe organ injury profile, comparable to that observed in KO mice (Fig. S5 F-M). These findings indicate that the microbiota and microbial metabolites are key mediators in ACE2-induced gut barrier repair.

Following the administration of ABX, we conducted a fecal microbiota transplantation (FMT) study on two groups of WT-ABX mice. Feces from WT or KO littermate mice were transplanted for a period of five consecutive days (Fig. 5A). Thereafter, the fecal samples from the recipients were collected for further analysis. Following the CLP operation, subjects who had received KO feces exhibited features of the KO mice. These included a diminished survival rate, hypoglycemia, a more pronounced inflammatory cytokine level, and weight loss (Fig. 5B–D and Fig. S6 A). Meanwhile, gut leak, bacterial translocation, and extra-intestinal organ injury were more severe in the KO recipients when compared to the mice that received WT feces (Fig. 5E–J and Fig. S6B-G). Additionally, we employed LC/MS to quantify 5-MTP levels post-ABX administration and FMT. Monitoring of parent-daughter ion pairs at m/z (233.1/146.1) and retention time of 5-MTP at 3.2 min (Fig. 5K) revealed a linear regression curve for peak area and standard concentration ($y = 7E\text{-}06x + 0.0204$, $R^2 = 0.99$). Following the depletion of the microbiota, 5-MTP was barely detected (tangerine curve). Mice that received feces from KO mice (pink curve) exhibited slightly higher 5-MTP content, while the 5-MTP levels of mice that received feces from WT mice (blue curve) recovered significantly (Fig. 5L, M). Further, the levels of 5-MTP in the feces of OE mice were found to be 2.3 times those observed in WT mice (Fig. S6H). These results demonstrated that the worsened features of KO mice in the septic challenge were transferable by the gut microbiome, and microbial metabolite 5-MTP was closely involved.

(See figure on next page.)

Fig. 5 The worsening of sepsis-induced gut leak is transferrable by fecal transplantation partially via 5-MTP. **A** A schematic diagram of fecal microbiota transplantation (FMT) and pretreatments. **B** Survival rates of WT-FMT mice and *Ace2*$^{-/y}$ -FMT mice underwent CLP ($n = 10$). **C**, **D** Serum glucose and TNF concentration of WT-FMT mice and *Ace2*$^{-/y}$ -FMT mice underwent CLP ($n = 6$). **E** Serum FD-4 concentration of WT-FMT mice and *Ace2*$^{-/y}$ -FMT mice underwent CLP ($n = 5$–9). **F**–**H** Ileal TJ protein (ZO-1 and OCLN) levels by Western blot ($n = 6$). **I** H&E staining (left panel), AB-PAS staining (middle panel), and IF staining of TJ protein OCLN (right panel) in the ileum. **J** Quantification of goblet cells ($n = 6$). **K** Typical multiple reaction monitoring chromatogram and chemical structural formula of pure 5-MTP. **L** Extracted ion chromatogram (XIC) overlap diagram targeting fecal 5-MTP of antibiotic (ABX) mice, WT-FMT mice, and *Ace2*$^{-/y}$ -FMT mice. **M** Fecal 5-MTP quantification of ABX-mice and FMT-mice ($n = 5$). Data are presented as the mean ± SD. $^{**}p < 0.01$, $^{***}p < 0.001$, and $^{****}p < 0.0001$ by two-tailed Student's *t* test or Mann–Whitney test. Intergroup survival differences were analyzed by a log-rank test. Abbreviations: ABX, antibiotic; FMT, fecal microbiota transplantation; PCT, procalcitonin; TNF, tumor necrosis factor; FD-4, fluorescein isothiocyanate-dextran; TJ, tight junction; OCLN, occludin; ZO-1, zona occludens 1; 5-MTP, 5-methoxytryptophan

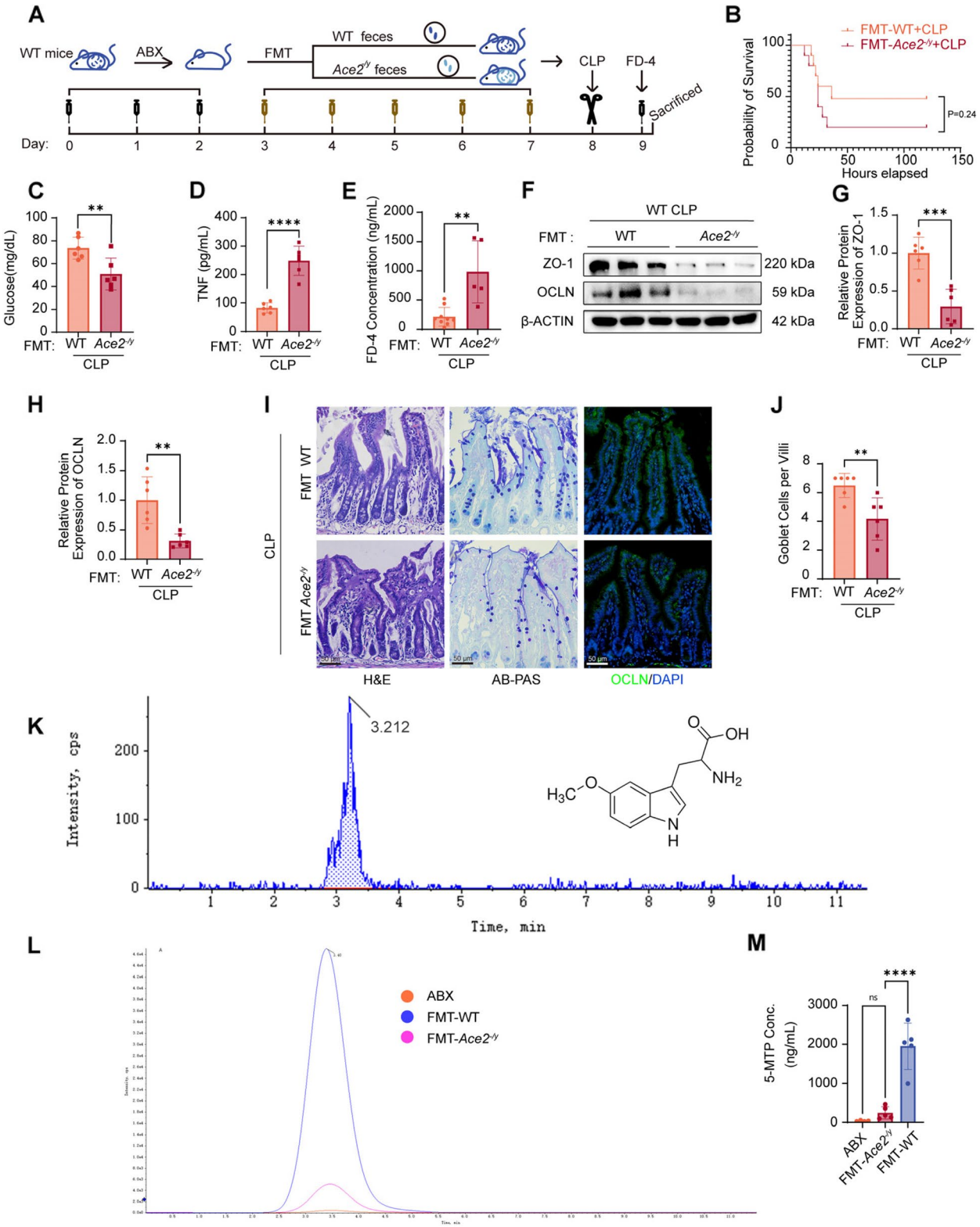

Fig. 5 (See legend on previous page.)

5-MTP-mediated gut barrier protection was associated with enhanced epithelial cell proliferation and the activation of the PI3K-AKT-WEE1 pathway

5-MTP was administered intraperitoneally to both WT mice and KO mice at 23.4 mg/kg [16] postoperation. The survival rate and body weight of the 5-MTP treatment group were significantly higher than the PBS group (Fig. 6A and Fig. S6I-K). Pro-inflammatory parameter levels were downregulated, while glucose levels were partly recovered (Fig. 6B–D and Fig. S6L, M). Gut leak and villi shattering were both alleviated, as indicated by serum FITC-dextran intensity and histological evaluation (Fig. 6E, F and Fig S6 N, O). Meanwhile, the inflammation of the alveoli and the thickening of the septa were less prominent in the lung than in the PBS-treated CLP group (Fig. 6G and Fig. S6P, Q). For renal tubular structure, a smoother brush border and a reduced degree of tubular dilation were observed (Fig. 6H and Fig. S6R, S). To investigate the mechanism of 5-MTP-induced gut barrier protection, transcriptional features were mapped (RNA-seq) for ileum from CLP mice treated with either 5-MTP or PBS ($n = 3$). KEGG pathway enrichment identified a cluster of genes concerning cell cycle and cell proliferation (Fig. S7 A). Therefore, an EdU assay was performed to measure cell proliferation. The nucleus of intestinal epithelial cells exhibited minimal staining with EdU in CLP mice, whereas increased EdU incorporation was observed in 5-MTP-treated mice (Fig. 6I). In accordance with the EdU assay, proliferating cell nuclear antigen (PCNA), a DNA synthesis marker, was upregulated in the ileum of 5-MTP-treated mice (Fig. 6 J). The effect of 5-MTP on proliferation was confirmed in the OE-CLP mice (Fig. S7B, C). The beneficial effect of 5-MTP on survival, weight change, glycemia, inflammation, gut leak, and epithelial cell proliferation could also be achieved by oral administration (Fig. S7D–K).

The PI3K-AKT signaling pathway, which is crucial for cell survival and proliferation [29, 30], was also enriched in the 5-MTP-treated group (Fig. 7A, Fig. S7L). Upregulation of the cyclin B1-CDK1 complex was revealed by the GO biological process and cellular component plot (Fig. 7B). The GSEA results and heatmap indicated that 5-MTP could induce intestinal epithelial cell repair by stimulating cell proliferation (Fig. 7C, D). We hypothesized that the mechanism was likely related to the PI3 K-AKT signaling pathway and the accelerated G2/M transition of the mitotic cell cycle. We performed qPCR to validate differentially expressed genes identified in RNA-seq as well as some other members of cyclin, cell division cyclin, and cyclin-dependent kinase families. The mRNA levels of *Ccnb1*, *Cdk1,* and cell cycle division 25B (*Cdc25B*) were found to be upregulated in the 5-MTP group, while *Ccna2* and *Cdc25 C* expression were downregulated (Fig. 7E). The expression of mitotic cell cycle-relevant genes was also validated in vitro (Fig. 7F). The expression of PI3 K, AKT, WEE1 (G2 checkpoint kinase), critical cell cycle kinases CDK1, CDK-tyrosine phosphatases CDC25B and CCNB1, and phosphorylated forms was examined (Fig. 7G). The activated PI3 K-AKT signaling pathway could phosphorylate WEE1, thereby preventing its phosphatase activity on CDK1. Furthermore, the upregulation of CDC25B could dephosphorylate P-CDK1, thereby activating the CDK1-CCNB1 complex and promoting the transition from the G2 to the M phase. The proportion of cells in the G1, S, and G2/M phases was quantified by flow cytometry (Fig. 7H, I). The administration of 5-MTP was found to overcome the cell cycle arrest at the G2/M phase induced by TNF (100 ng/ml). The pretreatment of cells with a CDK1 inhibitor (RO-3306) resulted in a diminished 5-MTP-induced G2/M phase release. Furthermore, as TNF exhibited a mild blockade of the cell cycle phase at G2/M, we proceeded to administer TNF + H_2O_2 (100 μM) in order to reproduce oxidative stress damage in sepsis. A greater proportion of cells was found to be blocked at the G2/M phase, with a distinct overturn observed in the 5-MTP-treated group (Fig. S7M, N).

(See figure on next page.)

Fig. 6 5-MTP protects the gut barrier by promoting epithelial cell proliferation. **A** Survival rates of sham or CLP mice treated with 5-MTP or phosphate-buffered saline (PBS) (n=5–10). **B**–**D** Serum TNF, PCT, and glucose concentration of CLP mice treated with 5-MTP or PBS (n=6). **E** Serum FD-4 concentration in CLP mice treated with 5-MTP or PBS (n=6). **F** Ileal H&E staining (left panel), AB-PAS staining (middle panel), and IF staining of TJ protein OCLN (right panel). The bar chart shows the quantification of ileal goblet cells (n=6). **G** H&E staining, histopathological evaluation, and the wet/dry ratio of the lungs (scale bar= 50 μm, n=4–6). **H** PAS staining, histopathological evaluation of the kidneys, and the serum creatinine levels of the mice (scale bar= 50 μm, n=4–6). **I** Quantification of ileal 5-ethynyl-20-deoxyuridine (EdU) assay of 5-MTP or PBS-treated CLP mice (scale bar= 50 μm, n=6). **J** Ileal proliferating cell nuclear antigen (PCNA) protein level by Western blot (n=6). **K** A schematic diagram illustrating the role of ACE2 in promoting intestinal epithelial cell repair in sepsis via the key microbial metabolite 5-MTP. Data are presented as the mean ± SD. ns=no significance, *$p < 0.05$, **$p < 0.01$, ***$p < 0.001$, and ****$p < 0.0001$ by two-tailed Student's t test or Mann-Whitney test. Intergroup survival differences were analyzed by the log-rank test. Abbreviations: 5-MTP, 5-methoxytryptophan; TNF, tumor necrosis factor; PCT, procalcitonin; FD-4, fluorescein isothiocyanate-dextran; Scr, serum creatinine

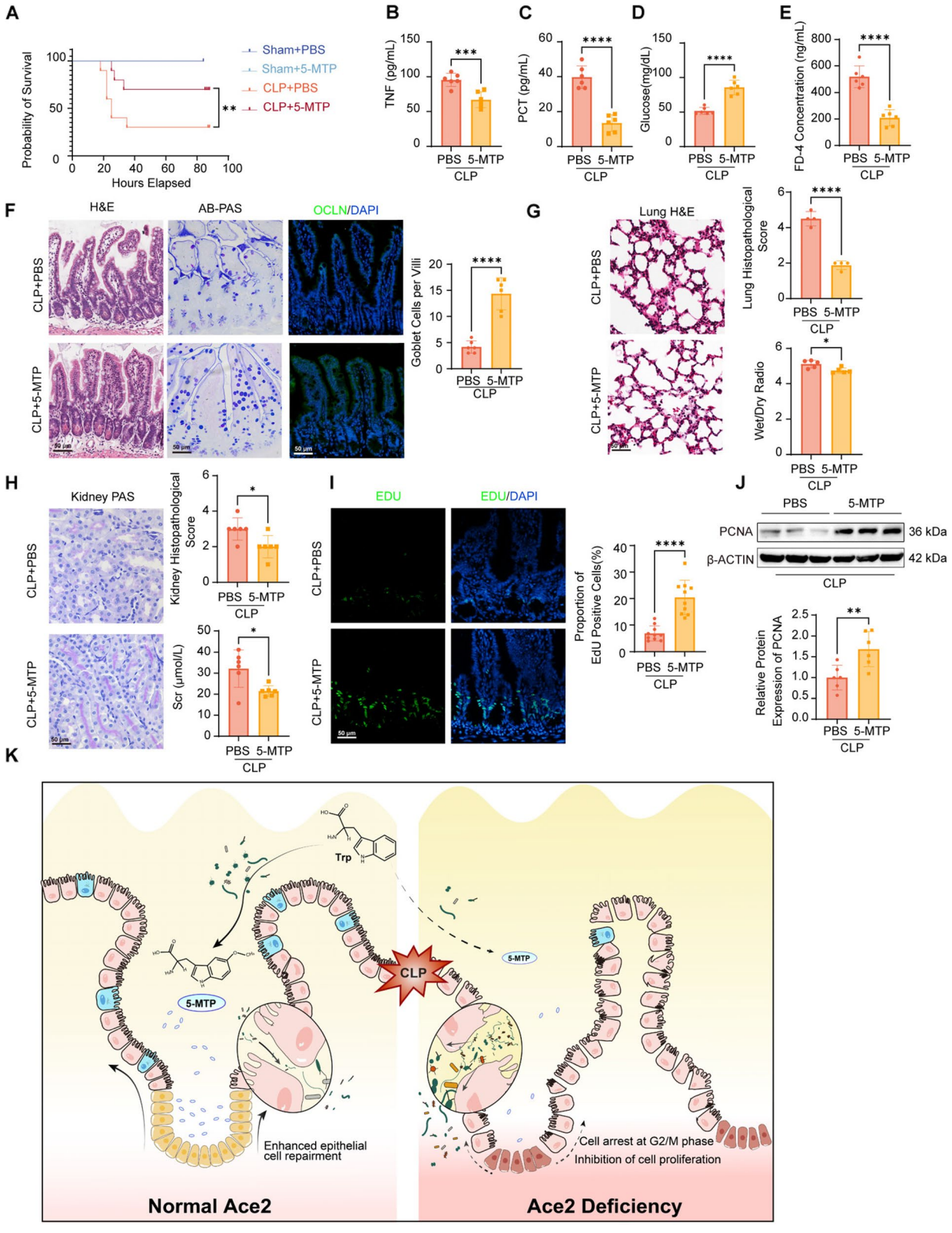

Fig. 6 (See legend on previous page.)

Discussion

In this study, we sought to examine the alterations in ACE2 expression in a murine model of sepsis. Our findings demonstrate that the shedding of ACE2 leads to an augmentation in gut leak, consequently impacting the function of vital organs and the survival status of septic mice. The specific mechanism may be to regulate the content of tryptophan metabolite 5-MTP produced by intestinal flora, which promotes the proliferation and repair of intestinal epithelial cells. Supplementation with 5-MTP can counteract the sepsis-induced barrier damage. The PI3K-AKT-WEE1 signaling pathway was identified as a key mediator of the beneficial effects of 5-MTP administration on the CDK1-CCNB1 complex. This resulted in a G2/M phase shift and enhanced epithelial repair.

ACE2 is a pivotal component of the renin-angiotensin system, which plays a multifaceted role in the vascular system, amino acid absorption, and SARS-CoV-2 entry. ACE2 shedding is the process by which the full-length membrane form of ACE2 (m-ACE2) undergoes ectodomain shedding to generate a soluble form (s-ACE2). This process has been demonstrated to be deleterious in diabetic cardiomyopathy (DCM) [31], neurons [32], and Influenza virus-infected airway epithelial cells [33]. Likewise, our study demonstrated that ACE2 shedding increases susceptibility to gut leak, facilitates bacteria translocation, and exacerbates organ dysfunction. As previously stated, the translocation of bacteria represents a pivotal link between localized intestinal injury and the onset of systemic inflammation. A method frequently employed to assess bacterial load is the cultivation of blood or tissue homogenization on agar plates [34]. In addition to this, in vivo imaging was performed to better visualize bacterial translocation. *Escherichia coli* was selected as the bioluminescent gene plasmid carrier due to its indigenous existence in the gut and its prevalence in the abdominal cavity in the CLP model [27]. A primary constraint of the CLP model is its reliance on the composition of the gut microbiota, which serves as the inoculum that initiates the infection. Consequently, it is imperative to demonstrate that the observed phenotype is not directly attributable to the altered gut microbiome in knock-out mice. By inoculation the same number of bacteria into the peritoneal cavity of mice, the intrinsic gut microbiota composition difference between WT and KO mice could be ruled out. Furthermore, we found that the shedding of ACE2 appears to exacerbate gut leak, at least in part, through the loss of the tryptophan metabolite 5-MTP. Tryptophan can be metabolized by the intestinal epithelium or intestinal flora [35]. To identify the major source of 5-MTP, a joint analysis of 16S rRNA sequencing and untargeted metabolomics was conducted, which revealed reduced levels of 5-MTP and a high correlation between this metabolite and specific bacterial species. Among these, reduced *Akkermansia muciniphila*, a mucin-degrading bacterium [36, 37], was consistent with the loss of mature goblet cells and the weakening of the mucus barrier in mice lacking ACE2. Furthermore, 5-MTP levels were almost non-existent in ABX-treated mice and could be reversed by FMT of conventional mouse feces. In addition, 5-MTP levels were increased in the feces of OE mice. These findings collectively indicated that 5-MTP is likely to be a microbial metabolite. Similarly, a study observed that the intestinal flora of mice with global overexpression of ACE2 (ACE2 KI) underwent modulation, with an increase in OTU abundance and α-diversity, and a significant upregulation of the tryptophan metabolism pathway [38].

To the best of our knowledge, this is the first study to reveal the function of fecal 5-MTP. The fecal 5-MTP level was found to be four times lower in *Ace2*-KO mice than in WT littermates. This high correlation between 5-MTP level and certain bacteria abundance was further verified by a series of FMT experiments and targeted metabolomics. Additionally, intestinal TPH-1 level was not altered by knocking out *Ace2*, suggesting that intestinal epithelial cells were unlikely responsible for 5-MTP synthesis in this context. Collectively, the loss of ACE2 resulted in a reduction in intestinal neutral amino acid transport, modification of the mucin environment, and, consequently, an impact on the abundance of tryptophan metabolizers. Previous studies have demonstrated that *Akkermansia muciniphila* and its outer protein Amuc_1100 regulate tryptophan metabolism [39]. It is therefore unsurprising that our joint analysis indicated that *Akkermansia muciniphila* was a promising bacterium in 5-MTP synthesis. However, further studies are required to gain a deeper understanding of the role

(See figure on next page.)

Fig. 7 The PI3K-AKT-WEE1 pathway participated in 5-MTP-induced epithelial cell proliferation and repair. **A**, **B** RNA-sequencing reveals enriched pathways and cellular components after 5-MTP administration. **C** Gene set enrichment analysis (GSEA) of regulated genes. **D** Heatmap visualizes regulated gene expression after 5-MTP administration ($n = 3$). **E** Cell cycle-related genes of CLP mice treated with 5-MTP or PBS were analyzed in ileal ($n = 5$). **F**, **G** Protein levels and mRNA levels of the cell cycle and PI3K-AKT-WEE1 signaling pathway were measured in vitro ($n = 6$–9). **H**, **I** Cell cycle analysis by flow cytometry ($n = 3$). Data are presented as the mean ± SD. ns = no significance, *$p < 0.05$, **$p < 0.01$, ***$p < 0.001$, and ****$p < 0.0001$ by two-tailed Student's *t* test or one-way ANOVA and Sidak's post hoc analysis

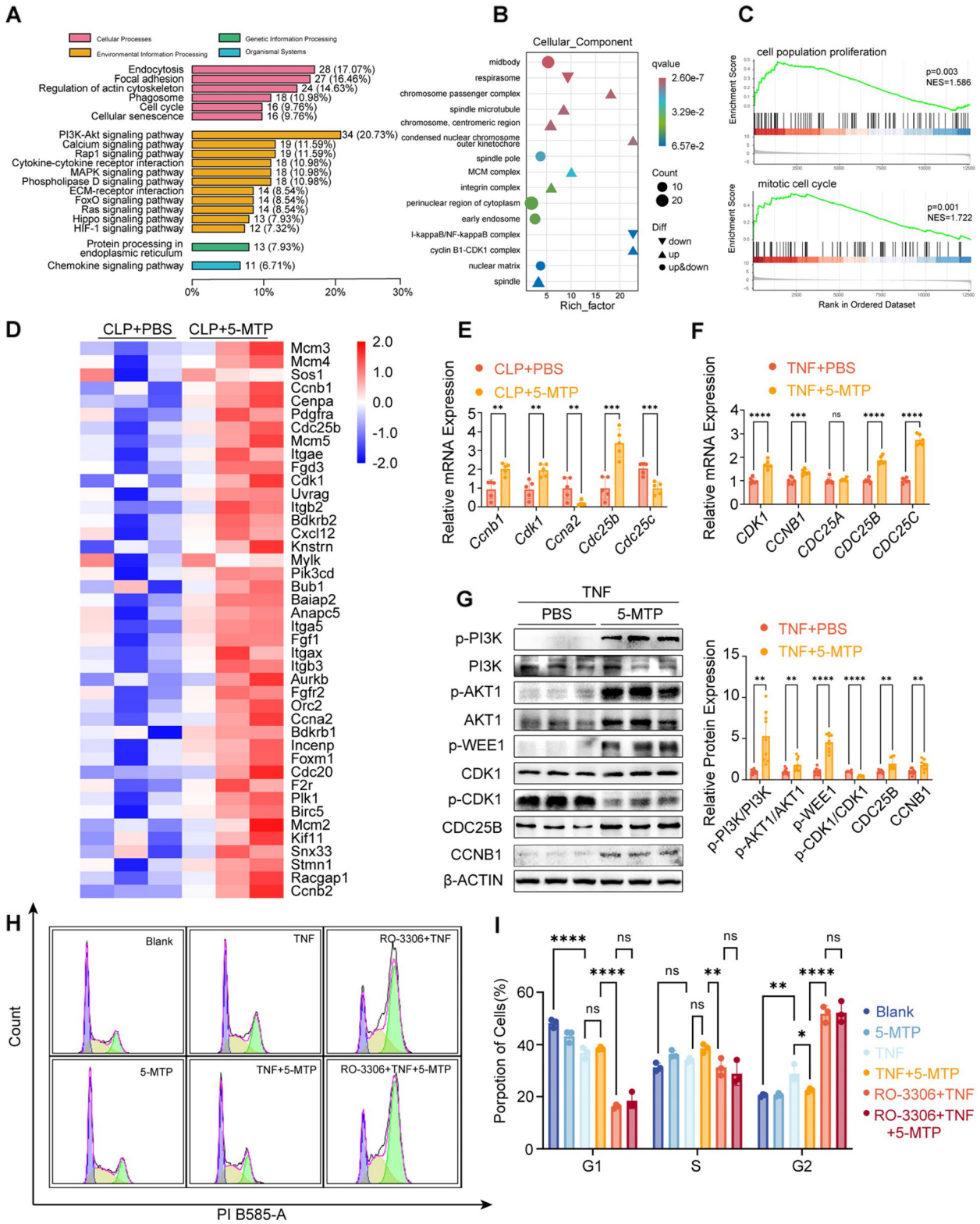

Fig. 7 (See legend on previous page.)

of other species in maintaining gut homeostasis. For instance, *Lactobacilli* has been demonstrated capable of converting tryptophan in the stomach and ileum of mice [40]. A specific species of this genus, *Ligilactobacillus murinus*, was also identified as highly correlated with the level of 5-MTP.

The limitations of our study are as follows. Firstly, in order to facilitate clinical transformation and application, OE mice were employed to rescue ACE2 shedding. However, this transgenic mouse model was of ICR background, rendering it incomparable with KO mice (C57 background). The baseline characteristics of the two strains of mice were demonstrated in Additional file 2. Furthermore, the generation of transgenic mice involved the microinjection of the mouse Ace2 promoter driving the human ACE2 coding sequence into the pronuclei of fertilized ova [20], resulting in variable copy numbers of the targeted sequence in the offspring. Therefore, we selected only KO mice and their WT littermates for microbial and metabolomics analysis. It would be more convincing to identify specific bacteria or metabolites in both KO and OE mice. Secondly, in septic mice, we observed a significant reduction in small intestine ACE2 levels, while other major ACE2-expressing organs remained unchanged. This suggests that the small intestine may be a primary source of s-ACE2. Further evidence could be provided by the utilization of villin-GFP reporter mice, which would strengthen this hypothesis.

Conclusions

Our findings demonstrate that ACE2 shedding contributes to gut leak and multiple organ dysfunction in sepsis. The mediator in question was found to be closely related to bacterial metabolite 5-MTP, a tryptophan derivative. Furthermore, the evidence indicates that 5-MTP promoted epithelial proliferation via the PI3K/AKT/WEE1 pathways and CDK1-CCNB1-induced G2/M cell cycle transition. Our study enriched the mechanisms by which ACE2 regulates gut homeostasis and shed light on further applications.

Abbreviations

AB-PAS	Alcian blue periodic acid Schiff
ABX	Antibiotic
ACE2	Angiotensin-converting enzyme 2
Ang	Angiotensin
ASV	Amplicon sequence variant
AUC	Area under the curve
BSA	Bovine serum albumin
CCK-8	Cell counting kit-8
CDC25B	Cell division cycle 25B
CFU	Colony-forming unit
CLP	Cecal ligation and puncture
DAPI	4′,6-Diamidino-2-phenylindole
DCM	Diabetic cardiomyopathy
DMEM	Dulbecco's modified Eagle medium
ECL	Enhanced chemiluminescence
EdU	5-Ethynyl-20-deoxyuridine
ELISA	Enzyme-linked immunosorbent assay
ESI	Electron spray ionization
FBS	Fetal bovine serum
FC	Fold change
FD-4	Fluorescein isothiocyanate-dextran
FITC	Fluorescein isothiocyanate
FMT	Fecal microbiota transplantation
FOV	Field of view
GO	Gene Ontology
H&E	Hematoxylin and eosin
HIOMT	Hydroxyindole O-methyltransferase
HRP	Horseradish peroxidase
IBIL	Indirect bilirubin
IF	Immunofluorescence
IHC	Immunohistochemistry
IL-6	Interleukin-6
KEGG	Kyoto Encyclopedia of Genes and Genomes
KO	Knockout
Lac	Lactic acid
LBP	LPS-binding protein
LEfSe	Linear discriminant analysis effect size
LPS	Lipopolysaccharide
m-ACE2	Membrane form of ACE2
MPO	Myeloperoxidase
OCLN	Occludin
OE	Overexpression
OTU	Operational taxonomic unit
PAS	Periodic acid Schiff staining
PBS	Phosphate-buffered saline
PCNA	Proliferating cell nuclear antigen
PCoA	Principal coordinate analysis
PCR	Polymerase chain reaction
PLF	Peritoneal lavage fluid
qPCR	Quantitative PCR
qRT-PCR	Quantitative real-time PCR
PCT	Procalcitonin
PLF	Peritoneal lavage fluid
pro-BNP	Pro-brain natriuretic peptide
ROC	Receiver operating characteristic
RPKM	Reads per kilobase per million mapped reads
s-ACE2	Soluble form of ACE2
Scr	Serum creatinine
SOFA	Sequential organ failure assessment
SPF	Specific pathogen-free
TBST	Tris-buffered saline with tween-20
TJ	Tight junction
TNF	Tumor necrosis factor
TPH	Tryptophan hydroxylase
WBC	White blood cell
WT	Wild type
XIC	Extracted ion chromatogram
5-MTP	5-Methoxytryptophan
ZO-1	Zona Occludens 1

Supplementary Information

The online version contains supplementary material available at https://doi.org/10.1186/s40168-025-02128-4.

Additional file 1. Figure S1. (A) Correlation analysis between ACE2 and the SOFA index (*n*=71). (B) Correlation analysis between LBP and the SOFA index (*n*=71). (C) Temporal gradient measurement of serum ACE2 levels (*n*=6). (D)Serum ACE2 levels of survivor and non-survivor in septic patients (n(survivor)=51, n(non-survivor) =20). (E) The ROC curve of ACE2 in predicting in-hospital mortality among patients(*n*=71). (F-G, I-J) Genotyping of *Ace2*$^{-/y}$ and hACE2$^{+/+}$ mice by agarose gel electrophoresis/ethidium bromide staining and IHC staining (Scale bar= 50 μm). (H) Changes in body weight of WT and *Ace2*$^{-/y}$ mice after undergoing CLP or sham surgery (*n*=4-6). (K-L) Feces and serum ACE2 levels of WT and

hACE2$^{+/+}$ mice underwent sham or CLP surgery(*n*=6). (M) Survival rates of WT and hACE2$^{+/+}$ mice underwent sham or CLP surgery (*n*=5-15). (N) Changes in body weight of WT and hACE2$^{+/+}$ mice after undergoing CLP or sham surgery (*n*=4-6). (O-Q) Serum glucose, TNF and PCT concentration of WT and hACE2$^{+/+}$ mice underwent sham or CLP surgery (*n*=4-6). (R) Serum FD-4 concentration of WT-sham, hACE2$^{+/+}$-sham, WT-CLP and hACE2$^{+/+}$-CLP mice(*n*=5-8). (S) Ileal TJ protein (OCLN and ZO-1) level by Western blot (*n*=4-6). (T) AB-PAS staining (upper panel), IF staining of TJ protein OCLN (middle panel), and H&E staining of ileum (Scale bar= 50 μm). (U) Quantification of ileal goblet cells(*n*=6). Data are presented as the mean ± SD. ns=no significance, *$p < 0.05$, **$p < 0.01$, ***$p < 0.001$, ****$p < 0.0001$ by one-way ANOVA and Sidak's post-hoc analysis. Intergroup survival differences were analyzed by Log-rank test. Abbreviations: SOFA, sequential organ failure assessment; LBP, lipopolysaccharide-binding protein; TNF, tumor necrosis factor; PCT, procalcitonin; FD-4, fluorescein isothiocyanate-dextran; TJ, tight junction; OCLN, occludin; ZO-1, zona occludens 1. Figure S2. (A-C) *In vivo* imaging and photon quantifications of bioluminescent *E. coli* of WT mice and hACE2$^{+/+}$mice after undergoing sham or CLP operation(*n*=3). (D-E) H&E staining, histopathological evaluation and wet/dry ratio of lungs (Scale bar= 50 μm, *n*=4-6). (F) PAS staining and histopathological evaluation of the kidneys (Scale bar= 50 μm, *n*=4-6). (G)Serum creatinine levels of the mice(*n*=6). (H) Survival rates of wild type (WT) mice after undergoing sham surgery or different doses of *E. coli* inoculation (*n*=4-10). (I) Survival rates of both wild type (WT) mice and *Ace2*$^{-/y}$ mice after undergoing sham or *E. coli* treatment (*n*=4-10). (J) Changes in body weight of WT and*Ace2*$^{-/y}$ mice after undergoing sham surgery or *E. coli* inoculation (*n*=4-6). (K-M) Serum glucose, TNF and FD-4 concentration of mice (*n*=4-6). (N) Ileal H&E staining and IF staining of TJ protein OCLN (Scale bar= 50 μm). Data are presented as the mean ± SD. ns=no significance, **$p < 0.01$, ***$p < 0.001$, ****$p < 0.0001$ by one-way ANOVA and Sidak's post-hoc analysis. Intergroup survival differences were analyzed by Log-rank test. Abbreviations: Scr, serum creatinine; TNF, tumor necrosis factor; FD-4, fluorescein isothiocyanate-dextran; TJ, tight junction; OCLN, occludin. Figure S3. (A, B) Quantification of bacterial load in blood, PLF and lung samples from mice underwent sham surgery or *E. coli* inoculation (n =3). (C-D) H&E staining, histopathological score and wet/dry ratio of lungs(*n*=4-6). (E)PAS staining and histopathological score of the kidneys (Scale bar= 50 μm, *n*=4-6). (F) Serum creatinine levels of the mice(*n*=6). Data are presented as the mean ± SD. ns=no significance, *$p < 0.05$, **$p < 0.01$, ***$p < 0.001$, ****$p < 0.0001$ by one-way ANOVA and Sidak's post-hoc analysis. Abbreviation: Scr, serum creatinine. Figure S4. (A) The multi-sample rarefaction curves and the rank abundance curve for all samples. (C-D) Taxonomic composition visualized by Krona online tool of WT and *Ace2*$^{-/y}$mice (*n*=4). (E-F) Western blot analysis of TPH1 protein levels in ileum (*n*=6-7). (G, H) Relative tryptamine and Indole abundance of WT and *Ace2*$^{-/y}$ mice (*n*=4). (I-K) Correlation analysis of 5-MTP levels and the abundance of linked bacterial species (*n*=8). (L)The relative abundance of linked bacterial species in WT and *Ace2*$^{-/y}$ mice (*n*=4). Data are presented as the mean ± SD. ns=no significance, *$p < 0.05$ by two-tailed Student's t test or Mann Whitney test. Abbreviations: TPH1, tryptophan 5-hydroxylase 1; 5-MTP, 5-methoxytryptophan. Figure S5. (A) Ileal H&E staining (upper panel), AB-PAS staining (middle panel) and IF staining of TJ protein OCLN (lower panel) in ABX-treated mice (Scale bar= 50 μm). (B) Serum FD-4 concentration of ABX-treated mice(*n*=5-6). (C) Quantification of goblet cells in ileum (*n*=6). (D-E) Western blot analysis of ileal TJs protein OCLN and ZO-1 level of ABX-treated mice(*n*=6). (F-G) Serum TNF and glucose concentration of ABX-treated mice (*n*=6). (H) Changes in body weight of ABX-treated WT and *Ace2*$^{-/y}$ mice after undergoing CLP or sham surgery(*n*=4-6). (I) *In vivo* imaging of ABX-treated WT mice and *Ace2*$^{-/y}$ mice after undergoing sham or CLP operation. (J-K) H&E staining, histopathological scores and wet/dry ratio of lungs of ABX-treated mice (Scale bar= 50 μm, *n*=4-6). (L) PAS staining and histopathological scores of kidneys of ABX-treated mice (Scale bar= 50 μm, *n*= 6). (M)Serum creatinine levels of ABX-treated mice(*n*=6). Data are presented as the mean ± SD. ns=no significance, **$p < 0.01$, ****$p < 0.0001$ by one-way ANOVA and Sidak's post-hoc analysis. Abbreviations: ABX, antibiotic; OCLN, occludin; ZO-1, Zona Occludens 1; TNF, tumor necrosis factor; Scr, serum creatinine. Figure S6. (A) Changes in body weight of WT-FMT mice and *Ace2*$^{-/y}$-FMT mice after undergoing CLP(*n*=6). (B) *In vivo*imaging and the and photon quantifications of bioluminescent *E. coli*of WT-FMT mice and *Ace2*$^{-/y}$-FMT mice after undergoing CLP operation(*n*=3). (C-E) H&E staining, histopathological evaluation and the wet/dry ratio of lungs from mice (Scale bar= 50 μm, *n*=4-6). (F)PAS staining and histopathological evaluation of kidneys from FMT CLP mice (Scale bar=50 μm, *n*=6). (G) Serum creatinine levels of the FMT CLP mice(*n*=6). (H) Feces 5-MTP levels of WT and hACE2$^{+/+}$mice (*n*=4). (I) Changes in body weight of WT-CLP mice treated with PBS or 5-MTP(*n*=6). (J) Survival rates of *Ace2*$^{-/y}$-CLP mice treated with PBS or 5-MTP(*n*=5-10). (K) Changes in body weight of *Ace2*$^{-/y}$-CLP mice treated with PBS or 5-MTP(*n*=6). (L-N) Serum glucose, TNF and FD-4 concentration of *Ace2*$^{-/y}$-CLP mice treated with PBS or 5-MTP (*n*=6). (O) H&E staining and IF staining of TJ protein OCLN in ileum (Scale bar= 50 μm). (P-Q) H&E staining, histopathological evaluation and the wet/dry ratio of lungs from *Ace2*$^{-/y}$-CLP mice (Scale bar= 50 μm, *n*=6). (R) PAS staining and histopathological scores of kidneys from *Ace2*$^{-/y}$-CLP mice (Scale bar= 50 μm, *n*=6). (S) Serum creatinine levels of *Ace2*$^{-/y}$-CLP mice(*n*=6). Data are presented as mean ± SD. *$p < 0.05$, **$p < 0.01$, ***$p< 0.001$, ****$p < 0.0001$ by two-tailed Student's t test or Mann Whitney test. Intergroup survival differences were analyzed by Log-rank test. Abbreviations: FMT, fecal microbiota transplantation; TNF, tumor necrosis factor; FD-4, fluorescein isothiocyanate-dextran; TJ, tight junction; OCLN, occludin; Scr, serum creatinine; 5-MTP, 5-methoxytryptophan. Figure S7. (A) Pathway enrichment and biological process of Gene Ontology (GO) enrichment analysis. (B) Ileal 5-ethynyl-20-deoxyuridine (EdU) assay of WT and hACE2$^{+/+}$ mice (Scale bar=50 μm). (C) Western blot analysis of Ileal PCNA protein levels in WT and hACE2+/+ mice (*n*=6). (D) Survival rates of sham or CLP mice treated with 5-MTP or PBS orally (*n*=5-10). (E)Changes in body weight of sham and CLP mice treated with PBS or 5-MTP orally(*n*=4-6). (F-H) Serum glucose, TNF and FD-4 concentration of mice treated with 5-MTP or PBS orally(*n*=4-6). (I) Ileal EdU assay (left panel) and IF staining of TJ protein OCLN (right panel) (Scale bar= 50 μm). (J) Ileal TJs protein OCLN level of mice by Western blot (*n*=6). (K) *In vivo* imaging of mice treated with PBS or 5-MTP orally. (L) GSEA analysis of PI3 K-AKT signaling pathway. (M, N) Flowcytometry cell cycle analysis of cells treated with 5-MTP (*n*=3). Data are presented as mean ± SD. *$p < 0.05$, **$p < 0.01$, ***$p < 0.001$, ****$p< 0.0001$ by two-tailed Student's t test, one-way ANOVA and Sidak's post-hoc analysis or Mann Whitney test. Intergroup survival differences were analyzed by Log-rank test. Abbreviations: PCNA, proliferating cell nuclear antigen; TNF, tumor necrosis factor; FD-4, fluorescein isothiocyanate-dextran; 5-MTP, 5-methoxytryptophan; TJ, tight junction; OCLN, occluding.

Additional file 2

Acknowledgements
We thank Dr. Ruo Huang of the Guangdong Provincial Key Laboratory of Gastroenterology, Nanfang Hospital for kindly providing a bioluminescent E. coli strain.

Authors' contributions
Xu Li, Ying Meng and Xi Liu contributed to the conception of the study; Jiacheng Gong and Haoyang Lu designed and performed the animal models, tissue sampling, histological staining, and molecular biology experiments; Yuhan Li and Qihan Xu performed the cellular intervention, data analysis and manuscript revision; Yuanyuan Ma contributed to histological evaluation and schematic diagram designing; Anni Lou, Wanfu Cui and Weihua Song contributed to clinical sample collections; Peng Qu, Zhuoer Chen and Linghao Quan contributed to manuscript preparation. The first four authors contributed equally to this work. The manuscript was collectively written and revised by Co-first authors, and the final version was approved by each of them.

Funding
This work was supported by the National Natural Science Foundation of China (82170641, 82470663, 82270089 and 81873583), Guangdong Provincial Science and Technology Projects (2021 A1515012595), Science and Technology Projects in Guangzhou (202201020206), National College Students'Innovation

and Entrepreneurship Training Program (202312121006), and President Foundation of Nanfang Hospital, Southern Medical University (2023 A041).

Data availability
No datasets were generated or analysed during the current study.

Declarations

Ethics approval and consent to participate
Human serum specimen collecting and medical records access were approved by the Ethics Committee of Nanfang Hospital, Southern Medical University (Approval Number: NFEC-2023–377).

Consent for publication
This manuscript does not contain data from any individual person.

Competing interests
The authors declare no competing interests.

Received: 26 June 2024 Accepted: 29 April 2025
Published online: 29 May 2025

References

1. Singer M, Deutschman CS, Seymour CW, Shankar-Hari M, Annane D, Bauer M, Bellomo R, Bernard GR, Chiche J-D, Coopersmith CM, et al. The third international consensus definitions for sepsis and septic shock (sepsis-3). JAMA. 2016;315(8):801–10.
2. Rudd KE, Johnson SC, Agesa KM, Shackelford KA, Tsoi D, Kievlan DR, Colombara DV, Ikuta KS, Kissoon N, Finfer S, et al. Global, regional, and national sepsis incidence and mortality, 1990–2017: analysis for the Global Burden of Disease Study. Lancet. 2020;395(10219):200–11.
3. Tirupakuzhi Vijayaraghavan BK, Adhikari NKJ. Sepsis epidemiology and outcomes in Asia: advancing the needle. Am J Respir Crit Care Med. 2022;206(9):1059–60.
4. Xie J, Wang H, Kang Y, Zhou L, Liu Z, Qin B, Ma X, Cao X, Chen D, Lu W, et al. The epidemiology of sepsis in Chinese ICUs: a national cross-sectional survey. Crit Care Med. 2020;48(3):e209–18.
5. Haussner F, Chakraborty S, Halbgebauer R, Huber-Lang M. Challenge to the intestinal mucosa during sepsis. Front Immunol. 2019;10:891.
6. Gomes RN, Teixeira-Cunha MGA, Figueiredo RT, Almeida PE, Alves SC, Bozza PT, Bozza FA, Bozza MT, Zimmerman GA, Castro-Faria-Neto HC. Bacterial clearance in septic mice is modulated by MCP-1/CCL2 and nitric oxide. Shock. 2013;39(1):63–9.
7. Hu J, Deng F, Zhao B, Lin Z, Sun Q, Yang X, Wu M, Qiu S, Chen Y, Yan Z, et al. Lactobacillus murinus alleviate intestinal ischemia/reperfusion injury through promoting the release of interleukin-10 from M2 macrophages via Toll-like receptor 2 signaling. Microbiome. 2022;10(1):38.
8. Mokhtari P, Metos J, Anandh Babu PV. Impact of type 1 diabetes on the composition and functional potential of gut microbiome in children and adolescents: possible mechanisms, current knowledge, and challenges. Gut Microbes. 2021;13(1):1–18.
9. Haak BW, Wiersinga WJ. The role of the gut microbiota in sepsis. Lancet Gastroenterol Hepatol. 2017;2(2):135–43.
10. Gong S, Yan Z, Liu Z, Niu M, Fang H, Li N, Huang C, Li L, Chen G, Luo H, et al. Intestinal Microbiota Mediates the Susceptibility to Polymicrobial Sepsis- Induced Liver Injury by Granisetron Generation in Mice. Hepatology. 2019;69(4):1751–67.
11. Camargo SM, Singer D, Makrides V, Huggel K, Pos KM, Wagner CA, Kuba K, Danilczyk U, Skovby F, Kleta R, et al. Tissue-specific amino acid transporter partners ACE2 and collectrin differentially interact with hartnup mutations. Gastroenterology. 2009;136(3):872–82.
12. Hashimoto T, Perlot T, Rehman A, Trichereau J, Ishiguro H, Paolino M, Sigl V, Hanada T, Hanada R, Lipinski S, et al. ACE2 links amino acid malnutrition to microbial ecology and intestinal inflammation. Nature. 2012;487(7408):477–81.
13. Duan Y, Prasad R, Feng D, Beli E, Li Calzi S, Longhini ALF, Lamendella R, Floyd JL, Dupont M, Noothi SK, et al. Bone Marrow-Derived Cells Restore Functional Integrity of the Gut Epithelial and Vascular Barriers in a Model of Diabetes and ACE2 Deficiency. Circ Res. 2019;125(11):969–88.
14. Prasad R, Floyd JL, Dupont M, Harbour A, Adu-Agyeiwaah Y, Asare-Bediako B, Chakraborty D, Kichler K, Rohella A, Li Calzi S, et al. Maintenance of Enteral ACE2 Prevents Diabetic Retinopathy in Type 1 Diabetes. Circ Res. 2023;132(1):e1–e21.
15. Roager HM, Licht TR. Microbial tryptophan catabolites in health and disease. Nat Commun. 2018;9(1):3294.
16. Wang YF, Hsu YJ, Wu HF, Lee GL, Yang YS, Wu JY, Yet SF, Wu KK, Kuo CC. Endothelium-derived 5-methoxytryptophan is a circulating anti-inflammatory molecule that blocks systemic inflammation. Circ Res. 2016;119(2):222–36.
17. Chen DQ, Cao G, Chen H, Argyopoulos CP, Yu H, Su W, Chen L, Samuels DC, Zhuang S, Bayliss GP, et al. Identification of serum metabolites associating with chronic kidney disease progression and anti-fibrotic effect of 5-methoxytryptophan. Nat Commun. 2019;10(1):1476.
18. Cheng HH, Kuo CC, Yan JL, Chen HL, Lin WC, Wang KH, Tsai KK, Guvén H, Flaberg E, Szekely L, et al. Control of cyclooxygenase-2 expression and tumorigenesis by endogenous 5-methoxytryptophan. Proc Natl Acad Sci USA. 2012;109(33):13231–6.
19. Yamamoto K, Ohishi M, Katsuya T, Ito N, Ikushima M, Kaibe M, Tatara Y, Shiota A, Sugano S, Takeda S, et al. Deletion of angiotensin-converting enzyme 2 accelerates pressure overload-induced cardiac dysfunction by increasing local angiotensin II. Hypertension. 2006;47(4):718–26.
20. Bao L, Deng W, Huang B, Gao H, Liu J, Ren L, Wei Q, Yu P, Xu Y, Qi F, et al. The pathogenicity of SARS-CoV-2 in hACE2 transgenic mice. Nature. 2020;583(7818):830–3.
21. Rittirsch D, Huber-Lang MS, Flierl MA, Ward PA. Immunodesign of experimental sepsis by cecal ligation and puncture. Nat Protoc. 2009;4(1):31–6.
22. Gong S, Yan Z, Liu Z, Niu M, Fang H, Li N, Huang C, Li L, Chen G, Luo H, et al. Intestinal microbiota mediates the susceptibility to polymicrobial sepsis-induced liver injury by granisetron generation in mice. Hepatology (Baltimore, MD). 2019;69(4):1751–67.
23. Fagerberg L, Hallström BM, Oksvold P, Kampf C, Djureinovic D, Odeberg J, Habuka M, Tahmasebpoor S, Danielsson A, Edlund K, et al. Analysis of the human tissue-specific expression by genome-wide integration of transcriptomics and antibody-based proteomics. Mol Cell Proteomics. 2014;13(2):397–406.
24. Otani S, Oami T, Yoseph BP, Klingensmith NJ, Chen CW, Liang Z, Coopersmith CM. Overexpression of BCL-2 in the Intestinal Epithelium Prevents Sepsis-Induced Gut Barrier Dysfunction via Altering Tight Junction Protein Expression. Shock. 2020;54(3):330–36.
25. Amatullah H, Shan Y, Beauchamp BL, Gali PL, Gupta S, Maron-Gutierrez T, Speck ER, Fox-Robichaud AE, Tsang JLY, Mei SHJ, et al. DJ-1/PARK7 impairs bacterial clearance in sepsis. Am J Respir Crit Care Med. 2017;195(7):889–905.
26. Soares MP, Teixeira L, Moita LF. Disease tolerance and immunity in host protection against infection. Nat Rev Immunol. 2017;17(2):83–96.
27. de Souza Gomes R, Navegantes-Lima KC, Monteiro VVS, de Brito Oliveira AL, Rodrigues DVS, Reis JF, Gomes ARQ, Prophiro JS, da Silva OS, Romão PRT, et al. Salivary Gland Extract from *Aedes aegypti* Improves Survival in Murine Polymicrobial Sepsis through Oxidative Mechanisms. Cells. 2018;7(11):182.
28. Kola G, Clifford CW, Campanaro CK, Dhingra RR, Dutschmann M, Jacono FJ, Dick TE. Peritoneal sepsis caused by Escherichia coli triggers brainstem inflammation and alters the function of sympatho-respiratory control circuits. J Neuroinflammation. 2024;21(1):45.
29. Thines L, Roushar FJ, Hedman AC, Sacks DB. The IQGAP scaffolds: Critical nodes bridging receptor activation to cellular signaling. J Cell Biol. 2023;222(6):e202205062.
30. He Y, Sun MM, Zhang GG, Yang J, Chen KS, Xu WW, Li B. Targeting PI3K/Akt signal transduction for cancer therapy. Signal Transduct Target Ther. 2021;6(1):425.
31. Xue F, Cheng J, Liu Y, Cheng C, Zhang M, Sui W, Chen W, Hao P, Zhang Y, Zhang C. Cardiomyocyte-specific knockout of ADAM17 ameliorates left ventricular remodeling and function in diabetic cardiomyopathy of mice. Signal Transduct Target Ther. 2022;7(1):259.
32. Parekh RU, Sriramula S. Activation of Kinin B1R upregulates ADAM17 and results in ACE2 Shedding in neurons. Int J Mol Sci. 2020;22(1):145.
33. Schweitzer KS, Crue T, Nall JM, Foster D, Sajuthi S, Correll KA, Nakamura M, Everman JL, Downey GP, Seibold MA, et al. Influenza virus infection

increases ACE2 expression and shedding in human small airway epithelial cells. Eur Respir J. 2021;58(1):2003988.
34. Gu P, Liu R, Yang Q, Xie L, Wei R, Li J, Mei F, Chen T, Zeng Z, He Y, et al. A metabolite from commensal Candida albicans enhances the bactericidal activity of macrophages and protects against sepsis. Cell Mol Immunol. 2023;20(10):1156–70.
35. Alexeev EE, Lanis JM, Kao DJ, Campbell EL, Kelly CJ, Battista KD, Gerich ME, Jenkins BR, Walk ST, Kominsky DJ, et al. Microbiota-derived indole metabolites promote human and murine intestinal homeostasis through regulation of interleukin-10 receptor. Am J Pathol. 2018;188(5):1183–94.
36. Rodrigues VF, Elias-Oliveira J, Pereira ÍS, Pereira JA, Barbosa SC, Machado MSG, Carlos D. Akkermansia muciniphila and gut immune system: a good friendship that attenuates inflammatory bowel disease, obesity, and diabetes. Front Immunol. 2022;13: 934695.
37. Everard A, Belzer C, Geurts L, Ouwerkerk JP, Druart C, Bindels LB, Guiot Y, Derrien M, Muccioli GG, Delzenne NM, et al. Cross-talk between Akkermansia muciniphila and intestinal epithelium controls diet-induced obesity. Proc Natl Acad Sci USA. 2013;110(22):9066–71.
38. Richards EM, Pepine CJ, Raizada MK, Kim S. The gut, its microbiome, and hypertension. Curr Hypertens Rep. 2017;19(4):36.
39. Gu Z, Pei W, Shen Y, Wang L, Zhu J, Zhang Y, Fan S, Wu Q, Li L, Zhang Z. Akkermansia muciniphila and its outer protein Amuc_1100 regulates tryptophan metabolism in colitis. Food Funct. 2021;12(20):10184–95.
40. Zelante T, Iannitti RG, Cunha C, De Luca A, Giovannini G, Pieraccini G, Zecchi R, D'Angelo C, Massi-Benedetti C, Fallarino F, et al. Tryptophan catabolites from microbiota engage aryl hydrocarbon receptor and balance mucosal reactivity via interleukin-22. Immunity. 2013;39(2):372–85.

Publisher's Note